

A-9873-MS

C.3

Los Alamos National Laboratory is operated by the University of California for the United States Department of Energy under contract W-7405-ENG-38.

CIC-14 REPORT COLLECTION  
REPRODUCTION  
COPY

*Collection of  $^{239}\text{Pu}$  Nuclear Data  
Revision 2 of ENDF/B-V*

LOS ALAMOS NATL. LAB. LIB.  
3 9338 00313 2148

**Los Alamos** Los Alamos National Laboratory  
Los Alamos, New Mexico 87545

This work was supported by the US Department of Energy, Office of Breeder Technology Projects.

DISCLAIMER

This report was prepared as an account of work sponsored by an agency of the United States Government. Neither the United States Government nor any agency thereof, nor any of their employees, makes any warranty, express or implied, or assumes any legal liability or responsibility for the accuracy, completeness, or usefulness of any information, apparatus, product, or process disclosed, or represents that its use would not infringe privately owned rights. Reference herein to any specific commercial product, process, or service by trade name, trademark, manufacturer, or otherwise, does not necessarily constitute or imply its endorsement, recommendation, or favoring by the United States Government or any agency thereof. The views and opinions of authors expressed herein do not necessarily state or reflect those of the United States Government or any agency thereof.

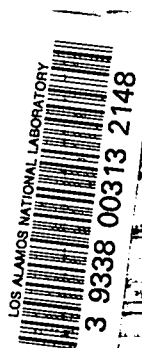
LA-9873-MS

UC-34c

Issued: October 1983

## Evaluation of $n + {}^{239}\text{Pu}$ Nuclear Data for Revision 2 of ENDF/B-V

E. D. Arthur  
P. G. Young  
D. G. Madland  
R. E. MacFarlane



**Los Alamos** Los Alamos National Laboratory  
Los Alamos, New Mexico 87545

EVALUATION OF  $n + {}^{239}\text{Pu}$  NUCLEAR DATA FOR  
REVISION 2 OF ENDF/B-V

by

E. D. Arthur, P. G. Young, D. G. Madland, and R. E. MacFarlane

ABSTRACT

A major revision of the ENDF/B-V evaluation of neutron-induced nuclear data for  ${}^{239}\text{Pu}$  has been completed. The most important changes to the evaluation include incorporation of a comprehensive new theoretical analysis based on recent experimental data to replace part of the total cross-section file and all of the elastic and inelastic cross sections and secondary distributions between  $\sim 10$  keV and 20 MeV; reevaluation of the prompt and total average neutron multiplicities from fission for incident energies between 0.4 and 11.5 MeV to correct discrepancies of almost 3% with new experimental data; and the replacement of all secondary neutron energy spectra from fission with improved shapes based on approximations to a new theoretical method. The evaluation has been tested by calculating various experimental results for five fast critical assemblies. Because major data types were either not thoroughly analyzed or were simply carried over from ENDF/B-V, this evaluation is regarded as an interim replacement until a more careful study can be done for ENDF/B-VI. The results of the new evaluation are being distributed as Revision 2 of ENDF/B-V by the National Nuclear Data Center at Brookhaven National Laboratory. A second version of the evaluation that includes a more complete description of the incident-energy-dependent fission neutron spectra has also been provided to the ENDF/A library at Brookhaven.

---

## I. INTRODUCTION

The ENDF/B-V evaluation for  $n + {}^{239}\text{Pu}$  was performed by Kujawski, Stewart, and LaBauve,<sup>1,2</sup> with major elements being provided by a task force of the Cross Section Evaluation Working Group. Due to the general unavailability of experimental data and limitations in theoretical techniques at that time, a major revision of the inelastic scattering files was not attempted. Since the issuance of ENDF/B-V, however, the inelastic data files have come into question, with the expectation being that at least some of the discrepancies between calculated and measured integral results<sup>3</sup> were being caused (or, at least, worsened) by the inelastic evaluation. Additionally, subsequent to the finalizing of ENDF/B-V, results from one of the main  $\bar{v}_p(E_n)$  experiments used for the evaluation were significantly revised above an incident neutron energy of 1 MeV.<sup>4</sup> Finally, a new method for calculating energy spectra of neutrons from fission<sup>5</sup> has become available that allows a more accurate representation of fission neutrons, yielding significant changes for  ${}^{239}\text{Pu}$  at secondary neutron energies above  $\sim 8$  MeV.

A new evaluation of  $n + {}^{239}\text{Pu}$  interactions that addresses the above problems has been prepared and distributed as Revision 2 of ENDF/B-V. A number of significant modifications were made to the original Version V data file. A comprehensive new theoretical analysis that utilizes several recent measurements was incorporated to describe the total, elastic, and inelastic scattering processes for incident neutron energies between  $\sim 10$  keV and 20 MeV. Extensive changes in the evaluated data files were required to reflect the new calculations, which differ significantly from ENDF/B-V. In addition, preliminary analyses were employed to correct the prompt and total neutron multiplicities from fission ( $\bar{v}_p$  and  $\bar{v}_t$ ) between 0.4 and 11.5 MeV (to conform with improved measurement results) and to improve the energy spectra of neutrons from fission at all energies (to reflect modern theoretical calculations). Because the latter analyses are preliminary and whole sections of Version V were adopted without revision, the present evaluation is regarded as interim until more thorough analyses are completed for Version VI. The theoretical and experimental bases for the revisions along with details of the changes to the ENDF/B-V data files are described in this report.

Section II summarizes the theoretical analysis used to upgrade the total, elastic, and inelastic data and provides detailed comparisons with the previous evaluation and with experimental data. The changes to  $\bar{v}_p$  and  $\bar{v}_t$  are described in Sect. III, which also includes comprehensive comparisons with experimental results. Section IV deals with the changes in representation of fission neutron spectra as a function of incident energy, using ENDF/B-V as a basis for comparison. Section V discusses the impact of these changes on integral calculations in reactor spectra and includes comparisons of calculated and experimental results for five critical assemblies. Finally, conclusions and recommendations for future work on the ENDF/B evaluation for  $^{239}\text{Pu}$  are given in Sect. VI.

## II. TOTAL, ELASTIC, AND INELASTIC NEUTRON DATA

### A. Theoretical Analysis

The basic theoretical components of the calculations are discussed in a paper by Arthur<sup>6</sup> at an inelastic scattering specialists meeting in Paris, and their application to  $^{239}\text{Pu}$  is described in a second paper presented at the Antwerp Conference.<sup>7</sup> Additional background material is available in several Los Alamos progress reports (Ref. 8, p. 15; Ref. 9, p. 28; Ref. 10, p. 18; and Ref. 11, p. 15).

The theoretical analysis involved application of two main reaction models: a coupled-channel optical model to describe direct-reaction contributions to inelastic scattering from collective states, and Hauser-Feshbach statistical theory to calculate compound-nucleus contributions to the reactions. The neutron transmission coefficients required for the Hauser-Feshbach calculations were obtained from the coupled-channel analysis, thereby ensuring consistency between the compound-nucleus and direct-reaction parts of the calculations. At incident energies above  $\sim 10$  MeV, preequilibrium theory was employed to correct the statistical theory calculations for nonequilibrium effects.

The ECIS<sup>12</sup> computer code was used for the coupled-channel deformed optical model calculations. The first six states of the <sup>239</sup>Pu ground state rotational band (1/2<sup>+</sup>, 3/2<sup>+</sup>, ..., 11/2<sup>+</sup>) were coupled in the calculation. The optical potential was represented in a standard manner,<sup>13</sup> and the coupling form factors needed in the expansion of the optical parameters were assumed complex. We used neutron optical parameters based on the Bruyères-le-Châtel analysis,<sup>14</sup> which relied mainly on fits to actinide total, elastic, and inelastic cross sections as well as s- and p-wave strength functions. Slight modifications were made to the optical parameters to produce better agreement with the <sup>239</sup>Pu total cross-section measurements of Poenitz et al.,<sup>15</sup> particularly around 1 MeV. The resulting optical and deformation parameters appear in Table I.

TABLE I

OPTICAL MODEL AND DEFORMATION PARAMETERS USED IN THE CALCULATIONS<sup>a</sup>

	r	a
	-----	-----
V = 46.2 - 0.3E	1.26	0.615
W <sub>SD</sub> = 3.6 + 0.4E	1.24	0.50
V <sub>SO</sub> = 6.2	1.12	0.47
β <sub>2</sub> = 0.21	β <sub>4</sub> = 0.065	

---

<sup>a</sup>The well depths and energies are in MeV; geometrical parameters are in fm.

The reaction theory code COMNUC<sup>16</sup> was used for the Hauser-Feshbach statistical theory calculations below 5 MeV, and the GNASH<sup>17</sup> code, which includes preequilibrium corrections, was employed at higher energies. Both codes utilized the phenomenological level density model of Gilbert and Cameron<sup>18</sup> along with the parameters of Cook.<sup>19</sup> A maximum amount of discrete level information was included for each nucleus appearing in the calculation. Such data were used to adjust the constant temperature level density parameters so as to reproduce the cumulative number of levels at low excitation energies while joining smoothly to the Fermi-gas form at higher energies. Gamma-ray transmission coefficients were calculated using a

Brink-Axel expression<sup>20,21</sup> that utilized two Lorentzian forms to represent the split giant dipole resonance. The gamma-ray transmission coefficients were normalized to reproduce measured  $2\pi\langle\Gamma_\gamma\rangle/\langle D\rangle$  data<sup>22</sup> available for s-wave resonances near the neutron binding energy.

Calculated elastic and inelastic scattering angular distributions for 0.7-MeV incident neutrons are shown in Fig. 1 with the experimental data of Haouat et al.<sup>14</sup> for the ground state band members of  $^{239}\text{Pu}$ . At this energy compound contributions can be significant, so that both the direct and compound-nucleus calculations are tested by this comparison. Overall, the agreement with experiment is good, although the calculation somewhat underpredicts the cross section for the  $7/2^+$  state.

Figure 2 presents a comparison of the calculated results with a scattering measurement by Smith and Guenther<sup>23</sup> for 2.5-MeV incident neutrons. This measurement includes elastic as well as inelastic neutrons from states in  $^{239}\text{Pu}$  up to an excitation energy of  $E_x = 0.2$  MeV. Smith and Guenther also used their results, together with total and fission cross-section data, to infer total inelastic scattering cross sections for levels above a given excitation-energy threshold. A comparison of our calculated inelastic cross sections (solid curve) with their inferred results is given in Fig. 3, with the excitation-energy threshold for the results ranging from  $E_x = 0.08$  to 0.3 MeV. This comparison provides indirect evidence of the validity of our assumption that inelastic scattering to states above the ground state rotational band is dominated by compound-nucleus effects, at least below 4 MeV. The dashed curve in Fig. 3 represents the ENDF/B-V evaluation, which lies substantially above both the experimental data and our calculations at higher energies.

Although we relied upon experimental data for the total fission cross section in the evaluation, the ability to calculate the fission channel reliably (better than  $\pm 5\%$ ) provides an important constraint on the Hauser-Feshbach calculation of other channels. For our calculation we introduced a double-humped fission model into the COMNUC and GNASH codes, using two uncoupled oscillators for the barrier representation with penetrabilities for each calculated from a Hill-Wheeler<sup>24</sup> expression.



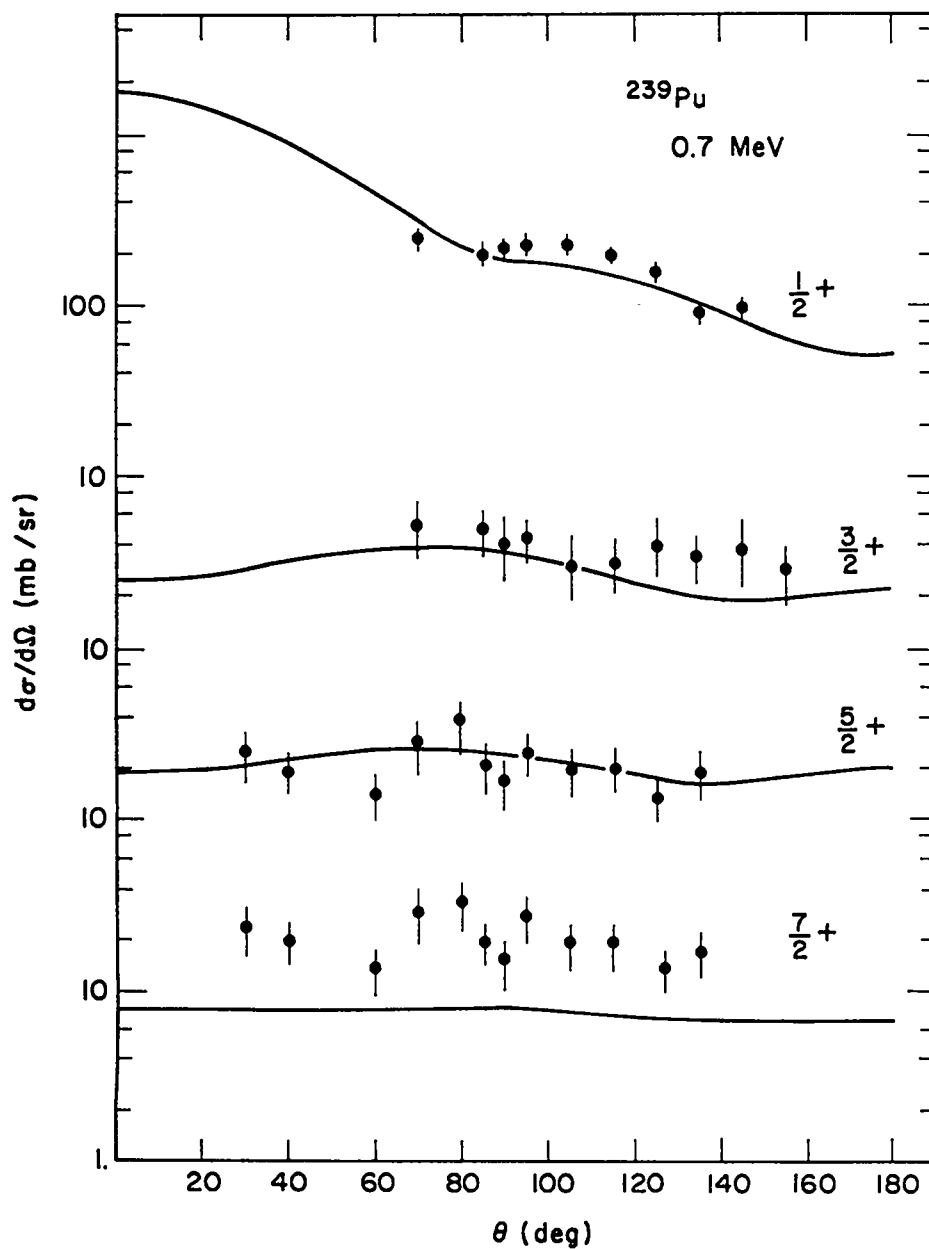


Fig. 1. Calculated angular distributions compared with recent measurements<sup>14</sup> of elastic and inelastic scattering on  $^{239}\text{Pu}$  at a neutron energy of 0.7 MeV.

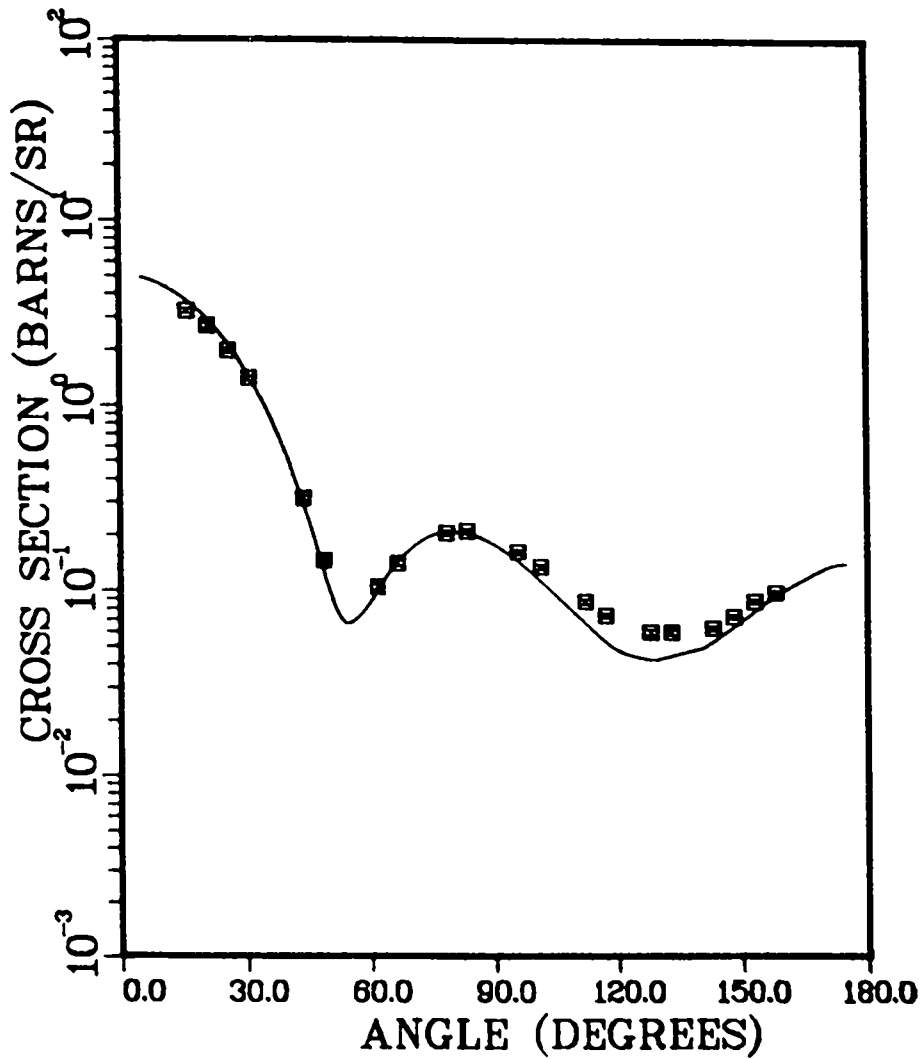


Fig. 2. Calculations of cross sections for scattering reactions that excite  $^{239}\text{Pu}$  states having energies  $\leq 200$  keV are compared with the data of Smith and Guenther<sup>23</sup> for 2.5-MeV incident neutrons.

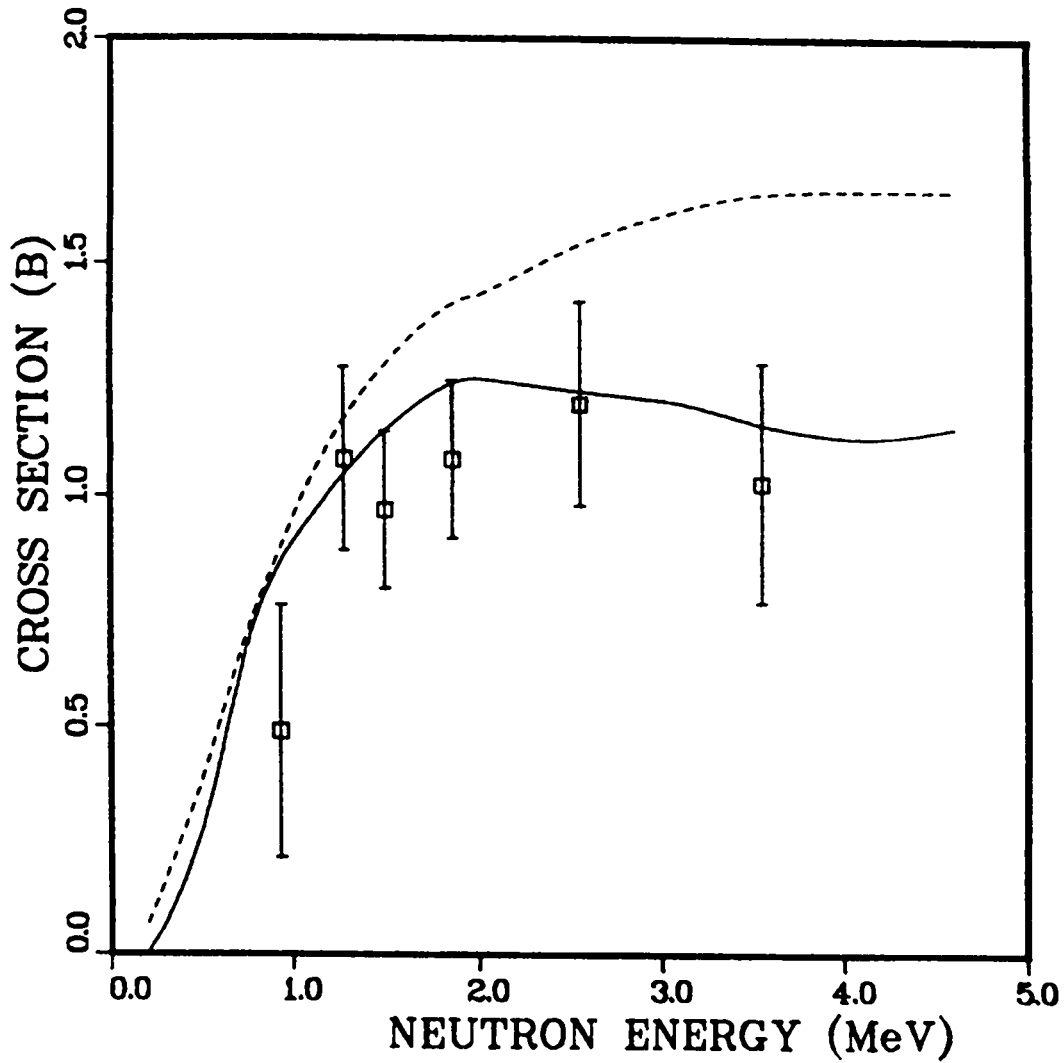


Fig. 3. Comparison of calculated inelastic cross sections (solid curve) for production of  $^{239}\text{Pu}$  states above a given excitation energy (0.08 - 0.3 MeV) with cross sections inferred from measurements by Smith and Guenther.<sup>23</sup> The dashed curve is ENDF/B-V.

In the case of first-chance fission, the spectrum of transition states occurring at each barrier was constructed from bandhead information<sup>25</sup> for the  $^{240}\text{Pu}$  compound system. At higher excitations, we assumed a continuum of transition states calculated with the Gilbert-Cameron level density expressions and parameters applicable for the ground state deformation case. We applied enhancements directly to these densities to account for deviations from symmetry present at each barrier. In addition to applying width-fluctuation corrections throughout the first-chance fission region, we also included corrections for Class II fluctuations based on the picket-fence approximation of Lynn et al.<sup>26</sup> These corrections are important primarily at low incident energies.

At higher incident neutron energies, multichance fission contributions [(n,nf), (n,2nf), etc.] introduce complications into Hauser-Feshbach calculations of the total fission cross section. Numerous fission parameters are required for the various compound nuclei involved, and shape uncertainties can be introduced into the total calculated fission cross sections due to unknowns associated with the energy behavior of the various components. Because higher energy Hauser-Feshbach calculations are time consuming and costly to perform, reliable fission parameter adjustments can be difficult to achieve, especially in the cases where insufficient information is available for parameter constraint.

To minimize these problems, we used, as independent sources of data, measurements<sup>27</sup> of direct-reaction fission probabilities ( $P_f$ ) and new data<sup>28</sup> on neutron-induced fission cross sections of  $^{238}\text{Pu}$ . These data sources allowed us to introduce additional constraints on barrier parameter determination for the  $^{239}\text{Pu}$  and  $^{238}\text{Pu}$  compound nuclei associated with second- and third-chance fission. In analyzing these data, we employed the same fission models used in our final calculations of the total  $n + ^{239}\text{Pu}$  fission cross sections. In the case of the  $P_f$  data, we accounted explicitly for spin population differences occurring between direct- and neutron-induced reactions.

An example of our fits to these data types appears in Fig. 4, where our calculated  $^{238}\text{Pu}(n,f)$  cross section is compared with the recent data of Budtz-Jørgensen et al.<sup>28</sup> In this case we did not attempt to optimize the fit

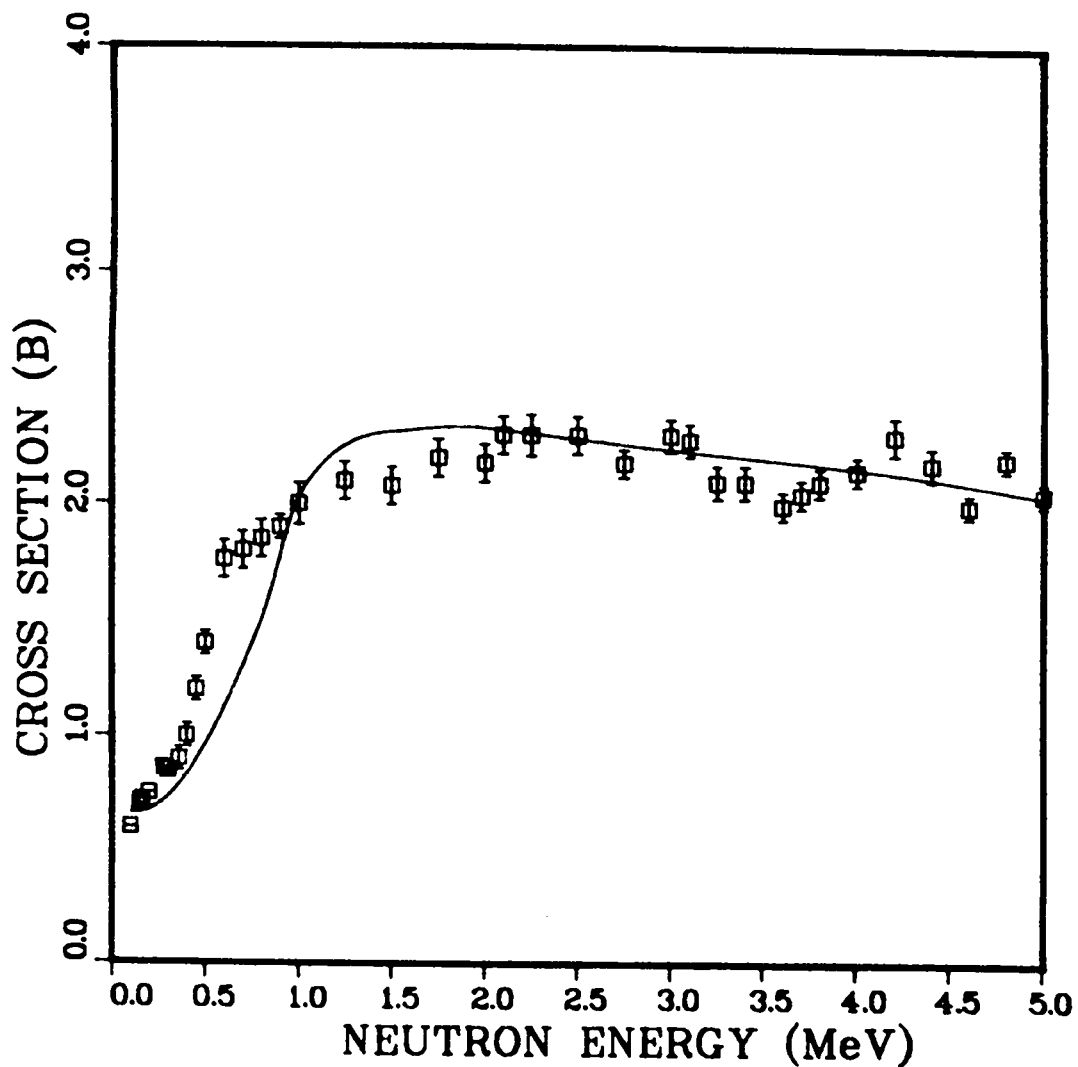


Fig. 4. Calculated  $^{238}\text{Pu}(n,f)$  cross sections used to obtain initial values for the  $^{239}\text{Pu}$  barrier parameters appearing in Table II are compared with the data of Budtz-Jørgensen et al.<sup>28</sup>

to the data below 0.1 MeV because our application of the barrier parameters to the  $^{239}\text{Pu}(n,n'f)$  reaction is not particularly sensitive to this behavior. The barrier parameters deduced from the data fit the onset of the  $^{239}\text{Pu}(n,n'f)$  cross section reasonably well (see below), but they disagree substantially with parameters required to fit  $P_f$  data determined from  $^{238}\text{Pu}(d,pf)$  measurements. We suspect this disagreement stems from problems in deuteron breakup corrections applied in the analysis of this reaction. More reliable  $P_f$  data exist for the  $^{238}\text{Pu}$  compound nucleus, as obtained through the  $^{237}\text{Np}(^3\text{He},df)$  reaction.\* Figure 5 shows our fit to these data after explicitly accounting for the spin population produced in the  $(^3\text{He},df)$  direct reaction.

The result of these analyses was a reliable set of starting barrier parameters for use in our  $n + ^{239}\text{Pu}$  calculations. Small adjustments were made in the parameters to optimize agreement with measured  $^{239}\text{Pu}(n,xf)$  data. The final parameters are summarized in Table II, which also includes the level density enhancements that were used. Note that the theoretical enhancements associated with these barrier shapes are  $\sigma\sqrt{8\pi}$  for the inner barrier and 2 for the outer one, where  $\sigma$  is the level density spin cutoff parameter. Figure 6 compares our calculated total  $^{239}\text{Pu}(n,xf)$  cross section (solid curve) with the data measured by Kari<sup>29</sup> between  $\sim 1$  and 16 MeV. The dashed and dotted curves illustrate the higher energy behavior that we calculate for the  $(n,n'f)$  and  $(n,2nf)$  contributions to the total fission cross section.

## B. Evaluation Results

A number of modifications were incorporated into the ENDF/B-V data file on the basis of the calculations described in the previous section.

1. The total cross section (MF=3; MT=1) was significantly modified in the range  $E_n = 0.025 - 1.5$  MeV.

---

\* H. C. Britt, Los Alamos National Laboratory, provided this information in September 1982.

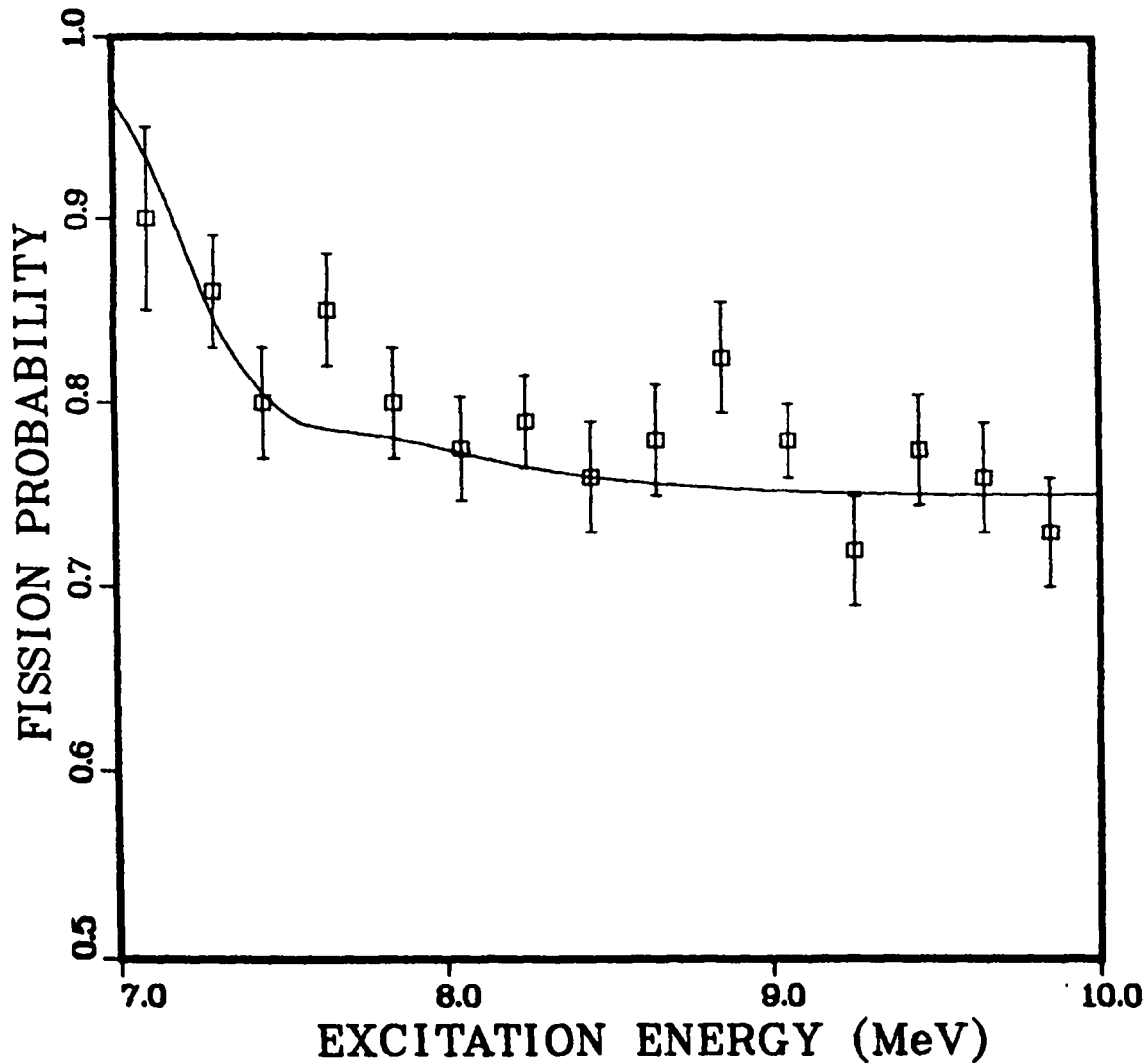


Fig. 5. Comparison of our fits with fission probabilities measured in the  $^{237}\text{Np}(^3\text{He},d)^{238}\text{Pu}(f)$  reaction. In these fits, which were used to determine the  $^{238}\text{Pu}$  barrier parameters of Table II, explicit account was taken of the compound-nucleus spin populations produced in this direct reaction.

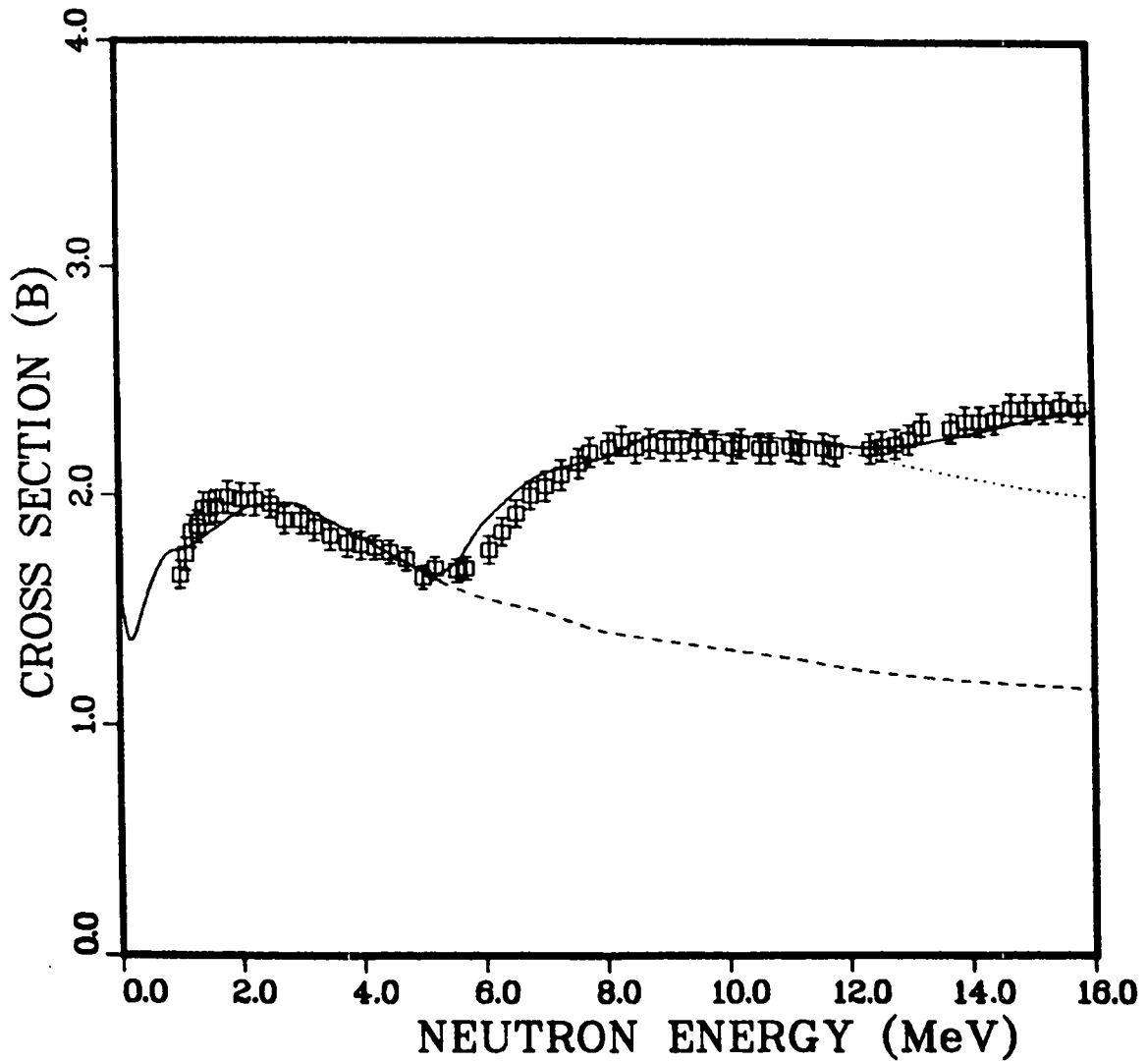


Fig. 6. Calculated  $n + {}^{239}\text{Pu}$  total fission cross sections (solid curve) compared with the data of Kari et al.<sup>29</sup> The dashed and dotted curves indicate the calculated behavior of the second-chance fission and the second- and third-chance fission sum.



2. The inelastic scattering cross sections and angular distributions (MF=3,4; MT=51-68) were completely replaced from threshold to 20 MeV.
3. The continuum inelastic cross section and secondary neutron energy spectra (MF=3,5; MT=91) were significantly revised to match the calculations.
4. The elastic cross section and angular distributions (MF=3,4; MT=2) were completely replaced from the inelastic threshold ( $E_n = 7.8932$  keV) to 20 MeV. (The actual elastic cross sections in the file were determined by subtracting the nonelastic cross section from the total, but these values were constrained by the analysis described above to closely approximate the theoretical results.)

TABLE II  
FISSION PARAMETERS FOR  $n + {}^{239}\text{Pu}$  CALCULATIONS<sup>a</sup>

		Barrier Height (MeV)	$h\omega$ (MeV)	Density Enhancement
${}^{240}\text{Pu}$	A	5.8	0.8	16
	B	5.45	0.6	2
${}^{239}\text{Pu}$	A	5.7	0.60	2.5
	B	5.05	0.50	2.5
${}^{238}\text{Pu}$	A	6.1	0.9	5
	B	5.55	0.85	2

---

<sup>a</sup>The isotopes appearing in the table are compound nuclei populated in the multichance fission of  $n + {}^{239}\text{Pu}$ . The inner and outer fission barriers are labeled A and B, respectively. The density enhancements shown are multiplied by  $U^{1/4}$  (where  $U$  is excitation energy,  $U > 1$ ) to obtain overall level density enhancements.

The newly evaluated total cross section below 2 MeV, which results directly from the analysis described in the previous section, is compared in Fig. 7 with the ENDF/B-V evaluation (dashed curve) and with experimental results. The lower energy cutoff of the curve (25 keV) is the upper boundary of the unresolved resonance region in ENDF/B-V, which we did not modify. The older data of Schwartz et al.<sup>30</sup> and Smith et al.<sup>31</sup> were available for Version V, but the more recent measurements of Poenitz et al.<sup>15</sup> were not. As mentioned above, the Poenitz data were considered in our theoretical calculations. As is evident in Fig. 7, significant modifications were made in the total cross-section evaluation between 25 and 500 keV, with changes as large as 7% being required.

The evaluated total cross section above 2 MeV is compared in Fig. 8 with the Poenitz et al. and Schwartz et al. measurements. Although some improvement in the total cross section is clearly possible, the ENDF/B-V evaluation was left unchanged in this energy range. There is, for example, nonphysical structure present in the evaluated curve at some energies.

The elastic cross section that results from our analysis is compared with ENDF/B-V (dashed curve) in Fig. 9 for incident energies in the range 0.025 to 20 MeV. The irregularities present in the revised evaluation are caused by structure in Version V nonelastic reactions [mainly (n, $\gamma$ ) and (n,f) reactions] that were not included in our modifications. Significant differences between ENDF/B-V and the revision occur at some energies, reaching ~11% near 1.6 MeV.

The evaluated inelastic excitation cross sections for the lowest 9 levels in  $^{239}\text{Pu}$  are compared with ENDF/B-V in Figs. 10-12. These comparisons illustrate the large differences that exist between the present (n,n') results and Version V, with discrepancies of factors greater than 2 being common. In the cases of the lowest 5 levels, the differences largely reflect the fact that direct reactions were included in our calculations but not in ENDF/B-V. For some of the levels, it also appears that shapes characteristic of lower spin states were assumed for the Version V results.

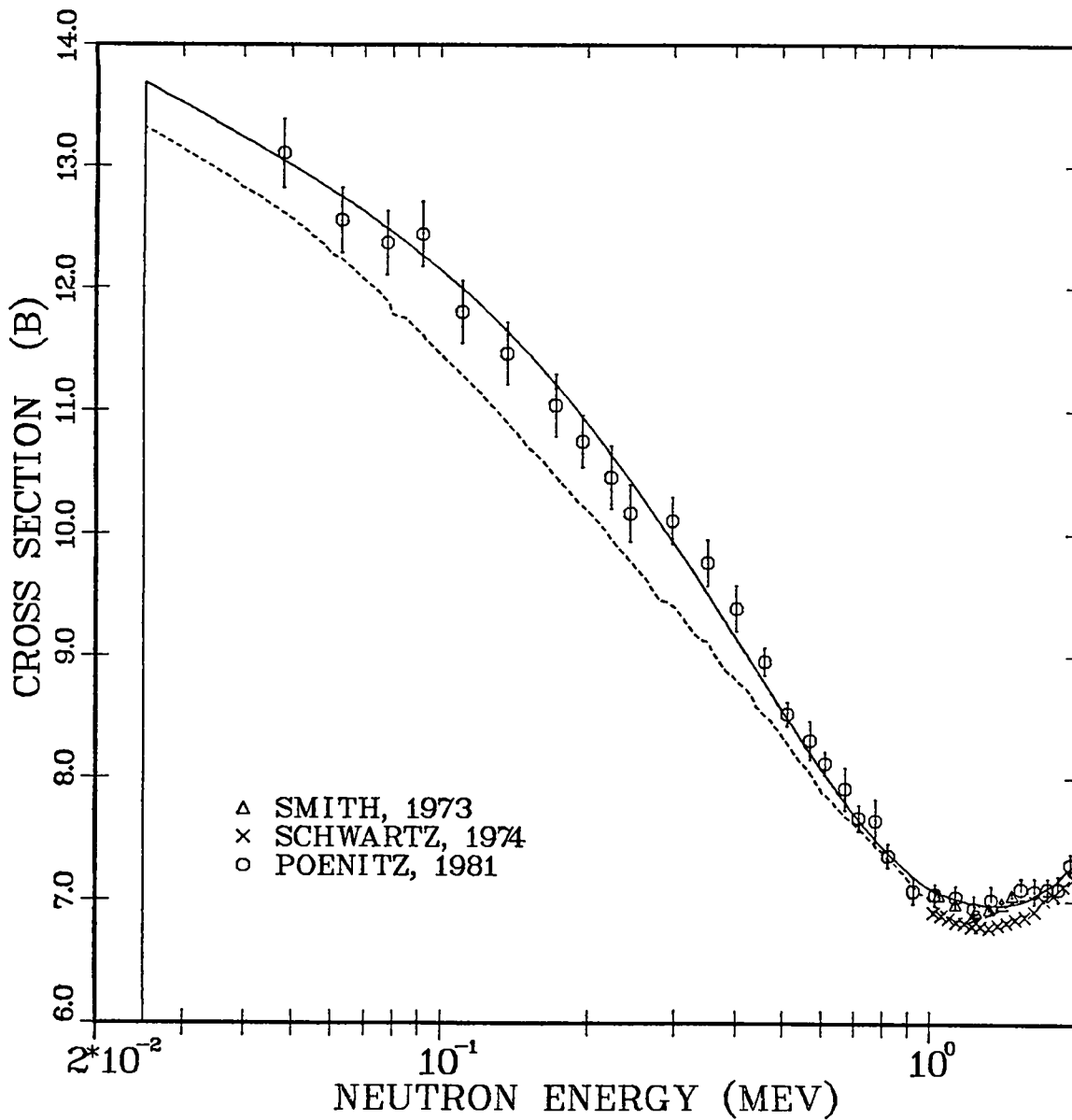


Fig. 7. Evaluated and measured<sup>15,30,31</sup> total cross sections for n +  $^{239}\text{Pu}$  interactions between 25 keV and 2 MeV. The solid curve is the present calculation, and the dashed curve is the ENDF/B-V evaluation.

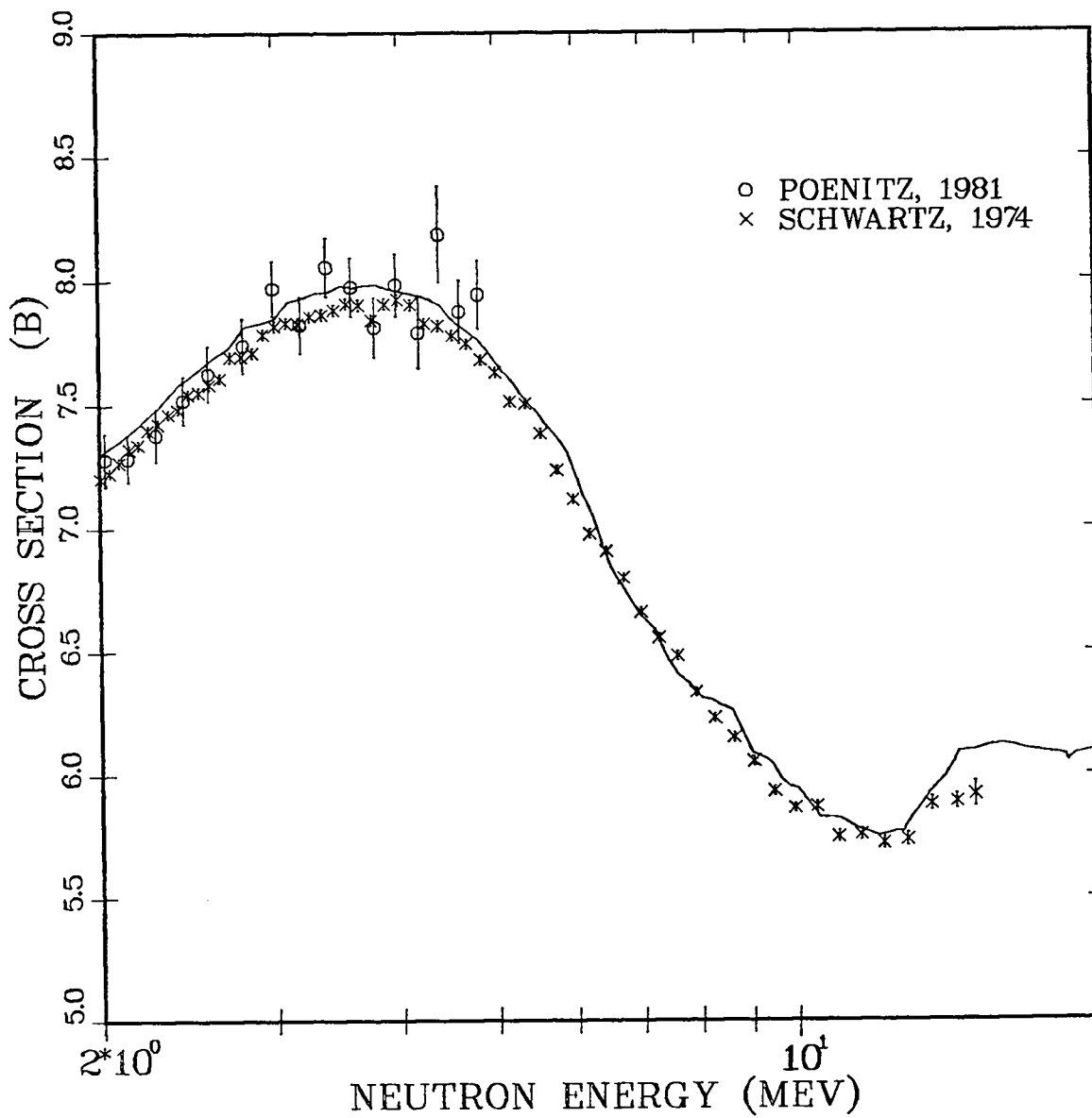


Fig. 8. Total cross section of  $^{239}\text{Pu}$  for neutron energies between 2 and 20 MeV. The points are experimental data,<sup>15,30</sup> and the solid curve represents both the present result and ENDF/B-V.

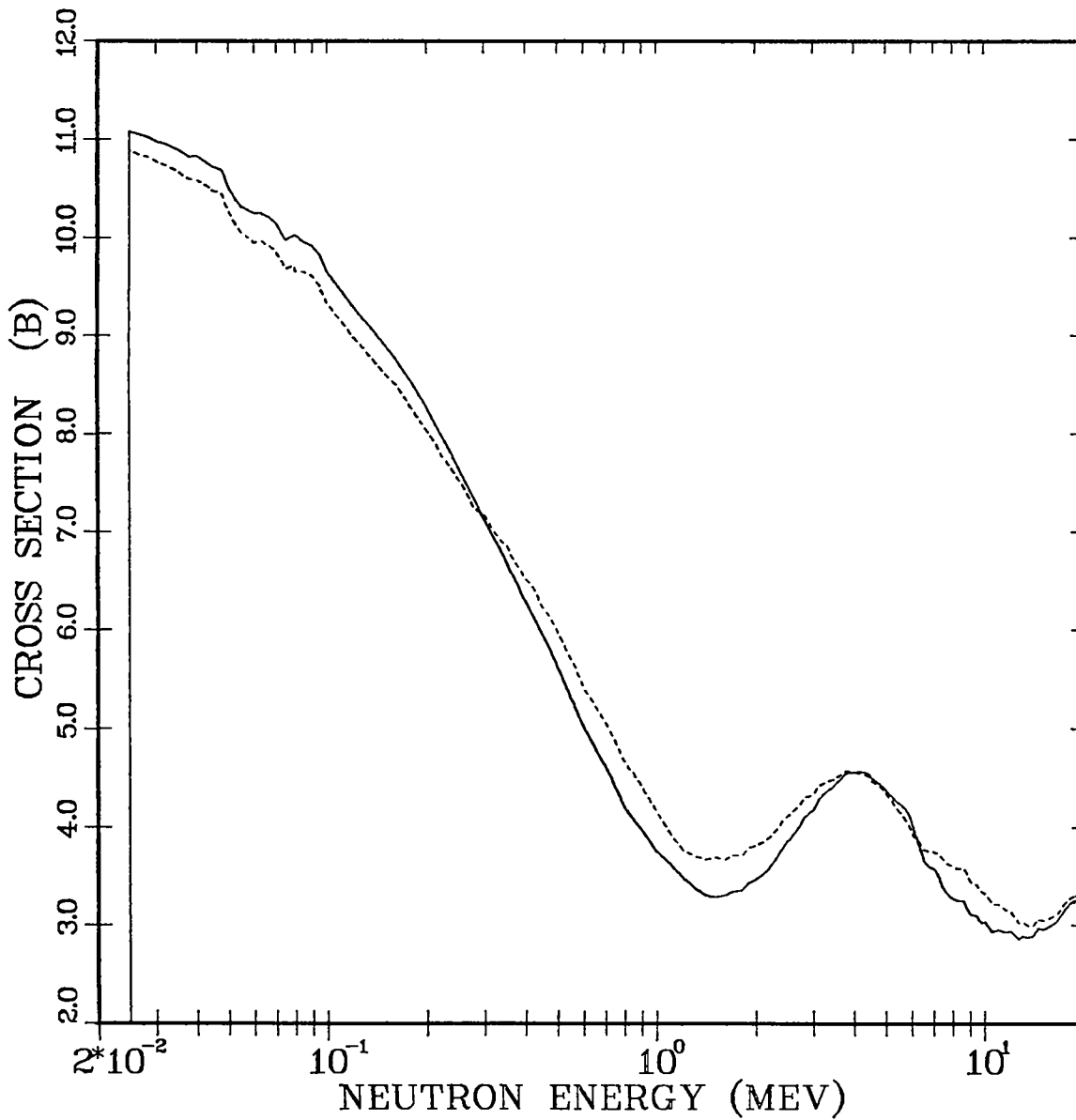


Fig. 9. Evaluated elastic cross sections for  $n + {}^{239}\text{Pu}$  between 20 keV and 20 MeV. The solid curve is the present revision, and the dashed curve is ENDF/B-V.

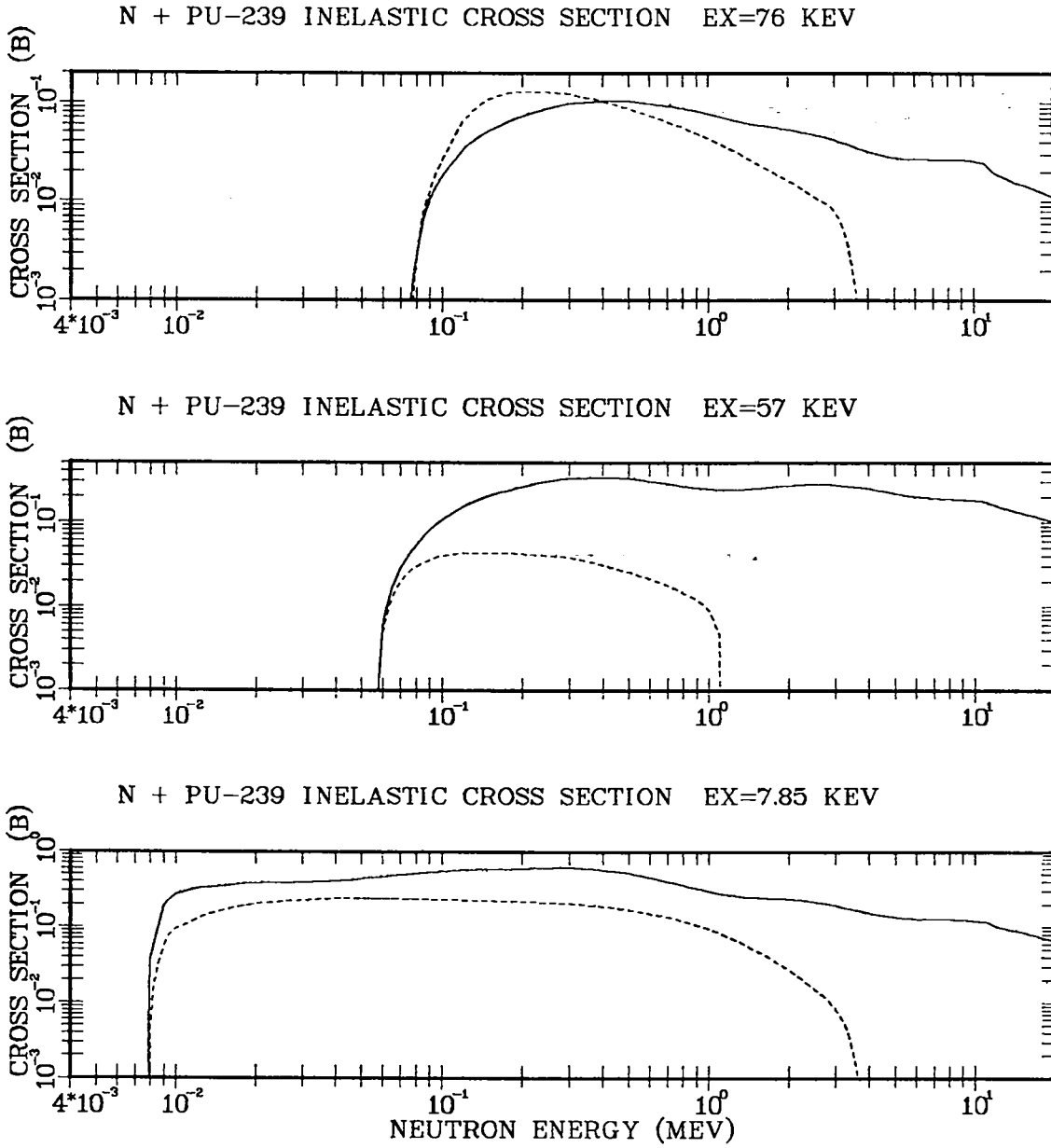


Fig. 10. Evaluated (n,n') excitation cross sections for the 1<sup>st</sup>, 2<sup>nd</sup>, and 3<sup>rd</sup> excited states of <sup>239</sup>Pu. The curves are defined in the caption of Fig. 9.

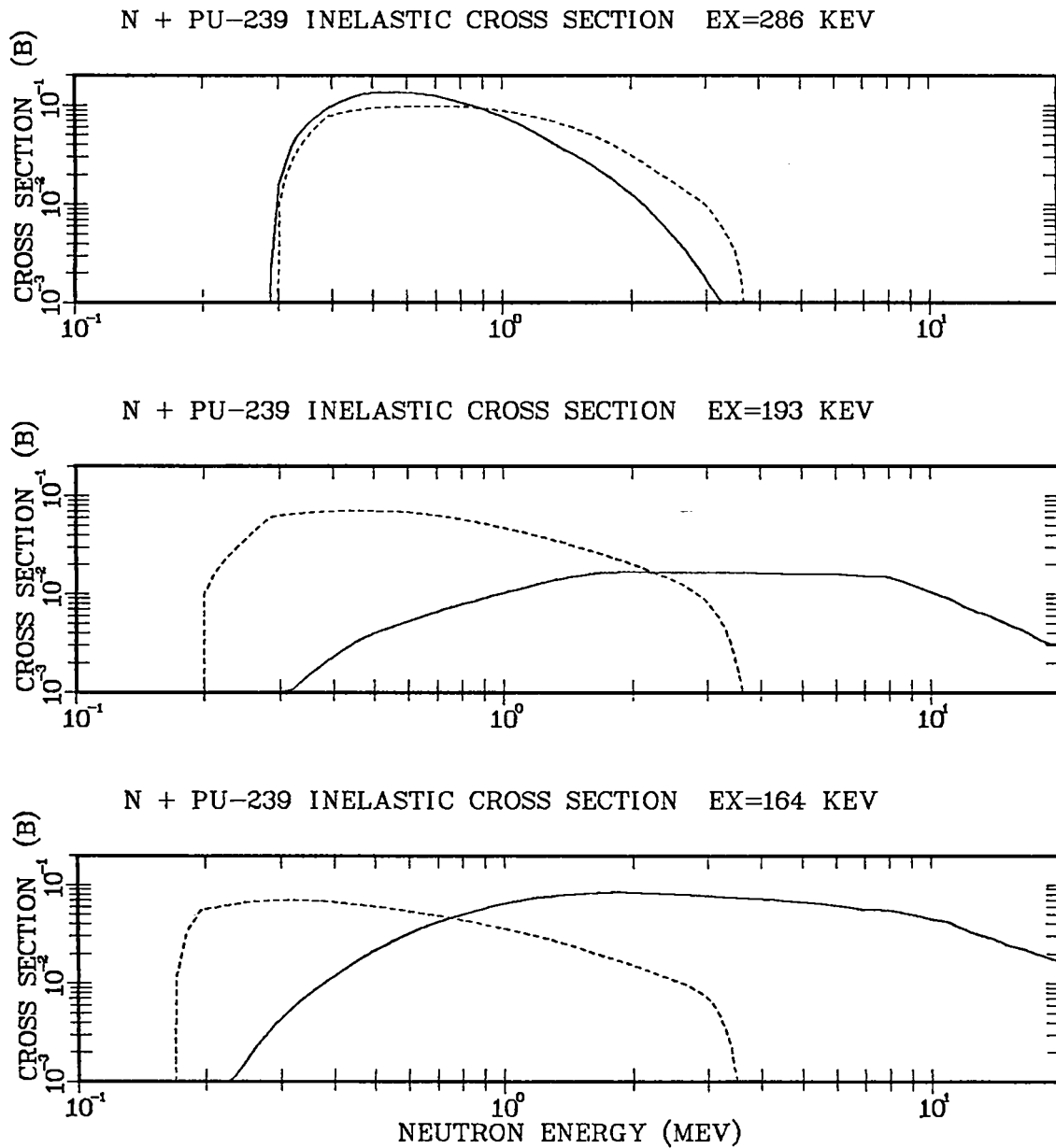


Fig. 11. Evaluated  $(n,n')$  excitation cross sections for the 4<sup>th</sup>, 5<sup>th</sup>, and 6<sup>th</sup> excited states of  $^{239}\text{Pu}$ . The curves are defined in the caption of Fig. 9.

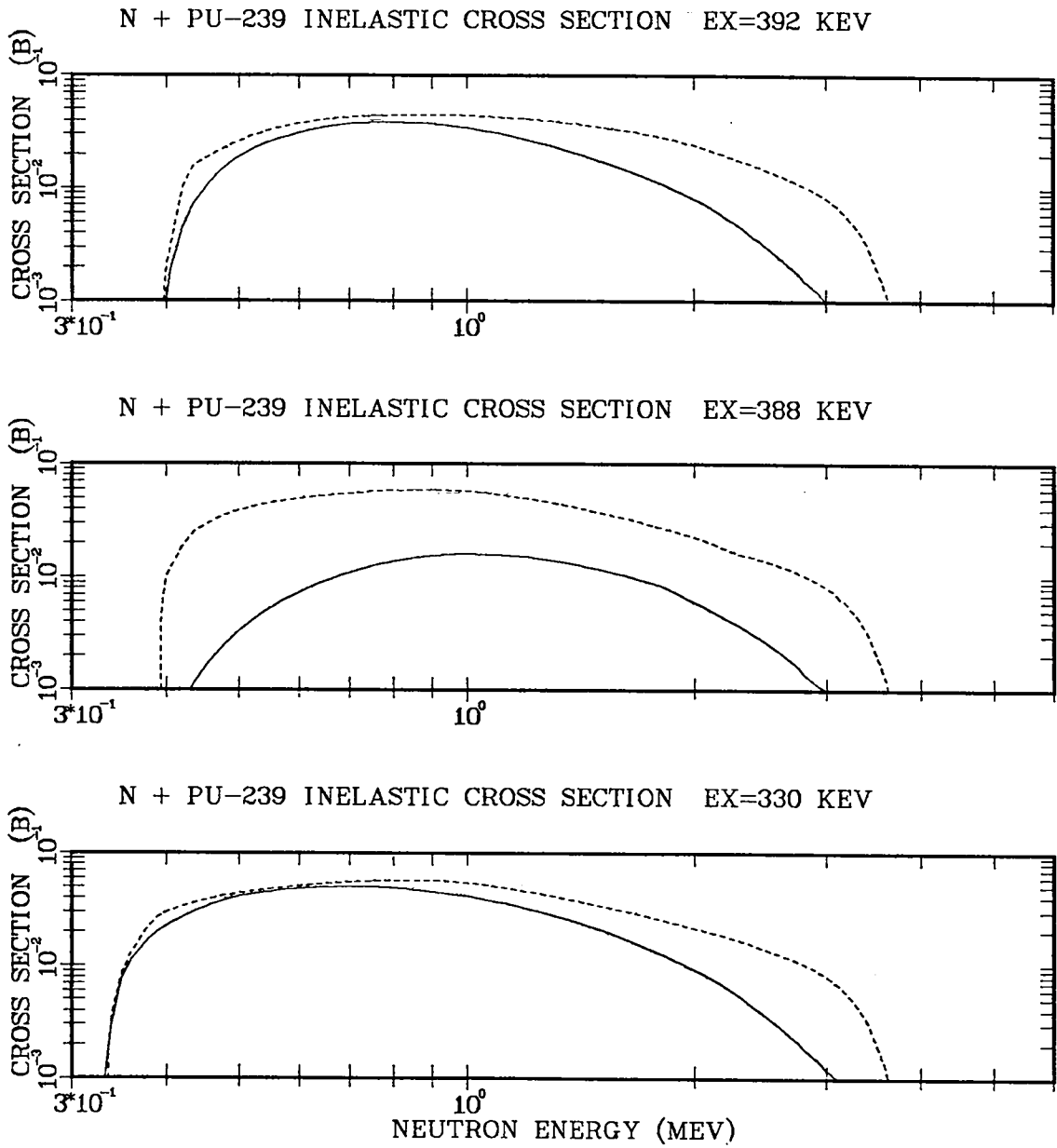


Fig. 12. Evaluated (n,n') excitation cross sections for the 7<sup>th</sup>, 8<sup>th</sup>, and 9<sup>th</sup> excited states of <sup>239</sup>Pu. The curves are defined in the caption of Fig. 9.



The overall effect on the total inelastic cross section of our revisions is shown by the comparison with ENDF/B-V in Fig. 13. Again, large differences from Version V (up to a factor of  $\sim 2$ ) are apparent, particularly over the energy range 0.01 to 1.0 MeV and above 7 MeV. The higher energy discrepancy, which is shown more clearly by the linear graph in the upper part of Fig. 13, is caused to a large extent by the inclusion of direct reaction and preequilibrium effects in the new calculations.

### III. PROMPT FISSION NEUTRON MULTIPLICITY

The ENDF/B-V evaluation of the prompt neutron multiplicity from fission,  $\bar{\nu}_p(E_n)$ , in the MeV range was influenced strongly by the experimental results of Frehaut et al.<sup>32,33</sup> These data resulted from a measurement reported earlier<sup>34</sup> that was revised to correct for suspected backgrounds thought to be higher than originally reported. In the years that followed publication of the "corrected" data, however, the background problem was studied further and the measurements repeated. The result is that the higher background was not confirmed, and final data from the experiments, including the new measurements, have been issued by Frehaut et al.,<sup>4</sup> showing significant disagreement ( $\sim \pm 1-3\%$ ) with ENDF/B-V in the MeV region.

In addition to the Frehaut results, a second  $\bar{\nu}_p(E_n)$  measurement of high accuracy ( $\sim \pm 0.5\%$ ) was completed by Gwin et al.<sup>35</sup> after the issuance of Version V. This new measurement, which covers the incident neutron energy range from below thermal to 10 MeV, is in substantial agreement with Frehaut's results above 1 MeV and with ENDF/B-V at lower energies (aside from the thermal region).

Of the older measurements, only one experiment (Savin et al.<sup>36</sup>) supports the now-withdrawn French results<sup>32</sup> and Version V in the 2-10 MeV region. The measurements of Hopkins and Diven,<sup>37</sup> Mather et al.,<sup>38</sup> and Condé et al.<sup>39</sup> are all consistent with the new results of Frehaut and Gwin et al. Therefore, as an interim correction before a more thorough variance-covariance analysis is made for Version VI of ENDF/B, we revised the Version V  $\bar{\nu}_p$  evaluation by constructing simple linear line segments that pass through the Frehaut and Gwin et al. data, joining Version V at 0.4 and 11.5 MeV, with a break in

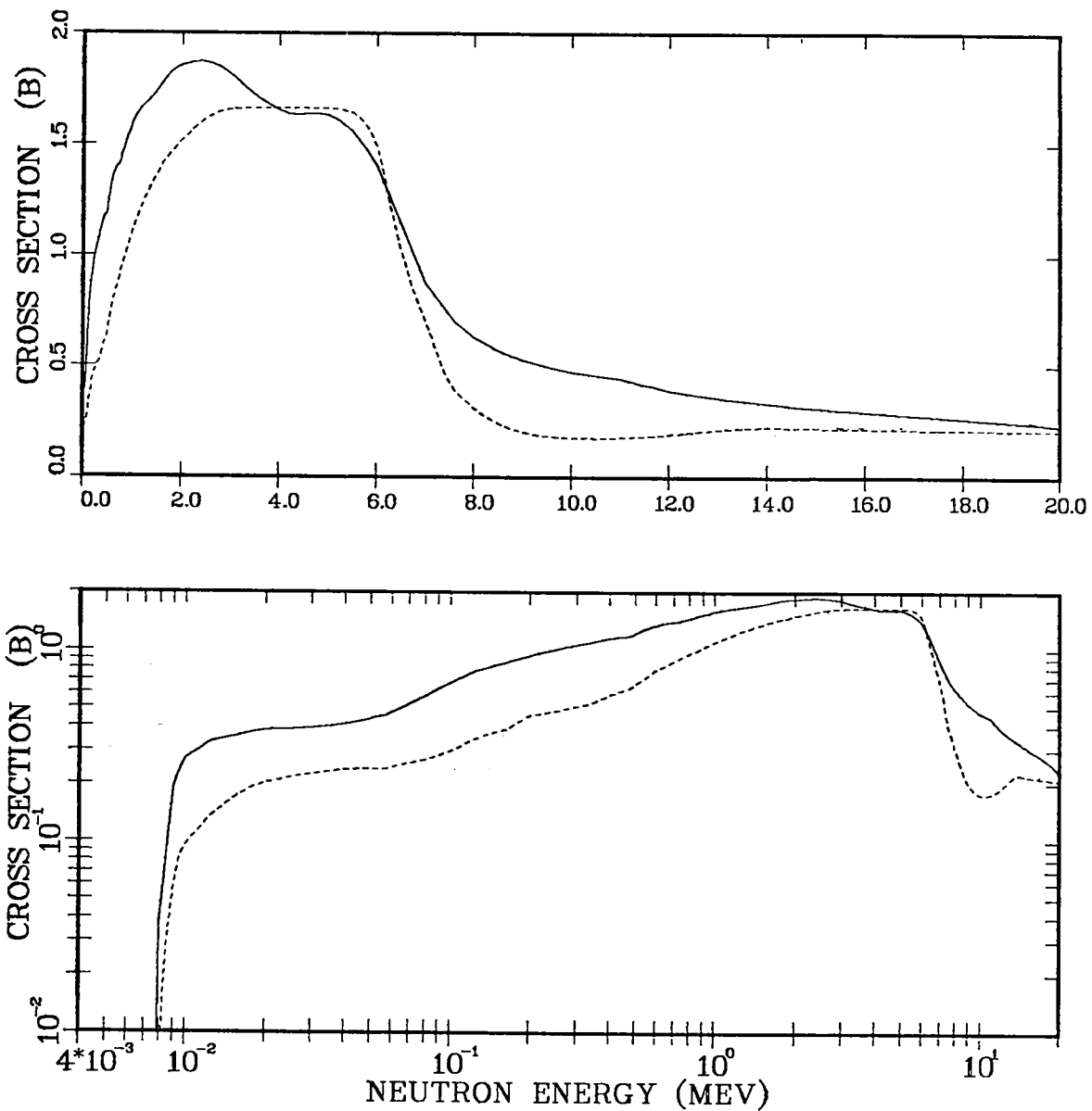


Fig. 13. Total inelastic neutron cross section for  $^{239}\text{Pu}$  from threshold to 20 MeV, shown on log-log and linear-linear scales. The solid curve is the present revision, and the dashed curve is ENDF/B-V.

slope at 3.6 MeV. The total neutron multiplicity ( $\bar{\nu}_t$ ) was also appropriately revised using the ENDF/B-V evaluation of delayed neutron multiplicities.

The revised  $\bar{\nu}_p(E_n)$  evaluation (solid curve) is compared in Fig. 14 with ENDF/B-V (dashed curve) and with the experimental data of Frehaut et al.<sup>4</sup> and Gwin et al.<sup>35</sup> between 0.1 and 10 MeV.\* Two different flight paths (20 and 85 m) were used in the Gwin measurements, and these are depicted by different symbols in Fig. 14. Figure 15 compares the evaluations over the same energy range with the older experimental data of Hopkins and Diven,<sup>37</sup> Mather et al.,<sup>38</sup> Conde' et al.,<sup>39</sup> and Savin et al.<sup>36</sup> As noted earlier, the Savin measurement is the only one that now supports Version V.

For completeness, the ENDF/B-V evaluation of  $\bar{\nu}_p(E_n)$ , which was left unchanged below 0.4 MeV, is compared in Fig. 16 with the lower energy portion of the Gwin measurements. Similarly, the Version V evaluation at energies above our revision (11.5 MeV) is compared in Fig. 17 with higher energy  $\bar{\nu}_p$  data. Especially in the case of the lower energy comparison, some revision of the evaluation appears to be warranted by the Gwin measurements. We have deferred such a revision, however, until a more careful study of data in the thermal region can be made, hopefully coupled through a variance-covariance analysis with other reactions and nuclei.

#### IV. NEUTRON ENERGY SPECTRA FROM FISSION

In 1982, an improved theoretical treatment for calculating neutron energy spectra from fission was published by Madland and Nix.<sup>5</sup> The two features of the new method that are most significant for applied data usage are that it permits use of physics information other than direct measurements in inferring fission neutron spectra, and it results in a more solidly grounded theoretical spectrum that differs from both the usual Maxwellian or Watt shapes used in data evaluations, particularly for secondary energies higher than  $\sim 8$  MeV.

---

\* All  $\bar{\nu}_p$  measurements relative to  $^{252}\text{Cf}$  were renormalized in our analysis using the value  $\bar{\nu}_p(^{252}\text{Cf}) = 3.758 \pm 0.004$  from Stehn et al.<sup>40</sup>

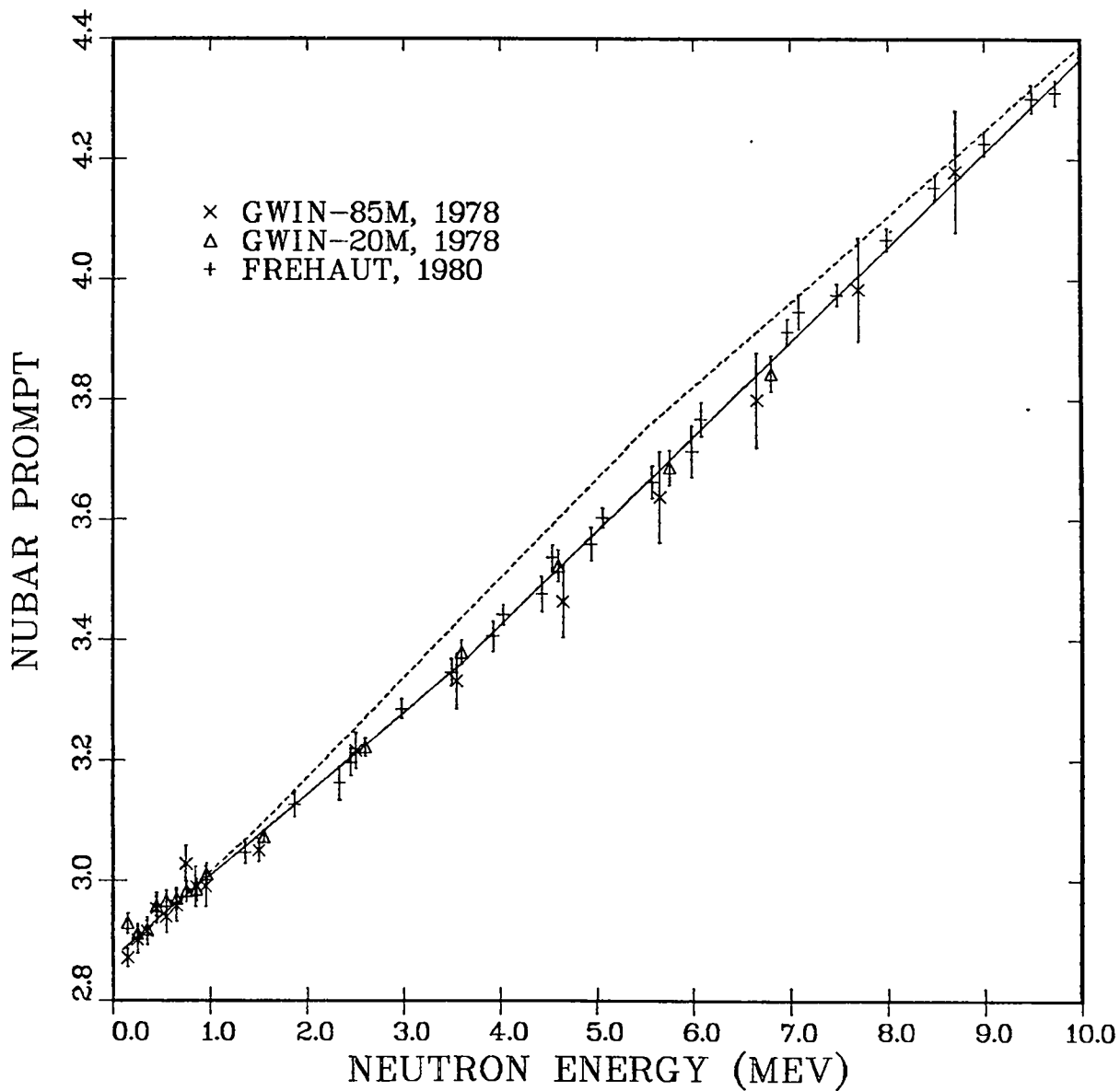


Fig. 14. Evaluated prompt fission multiplicity  $\bar{\nu}_p(E_n)$  between  $E_n = 0.1$  and 10 MeV compared with the experimental data of Gwin et al.<sup>35</sup> and Frehaut et al.<sup>4</sup> The curves are defined in the caption to Fig. 13.

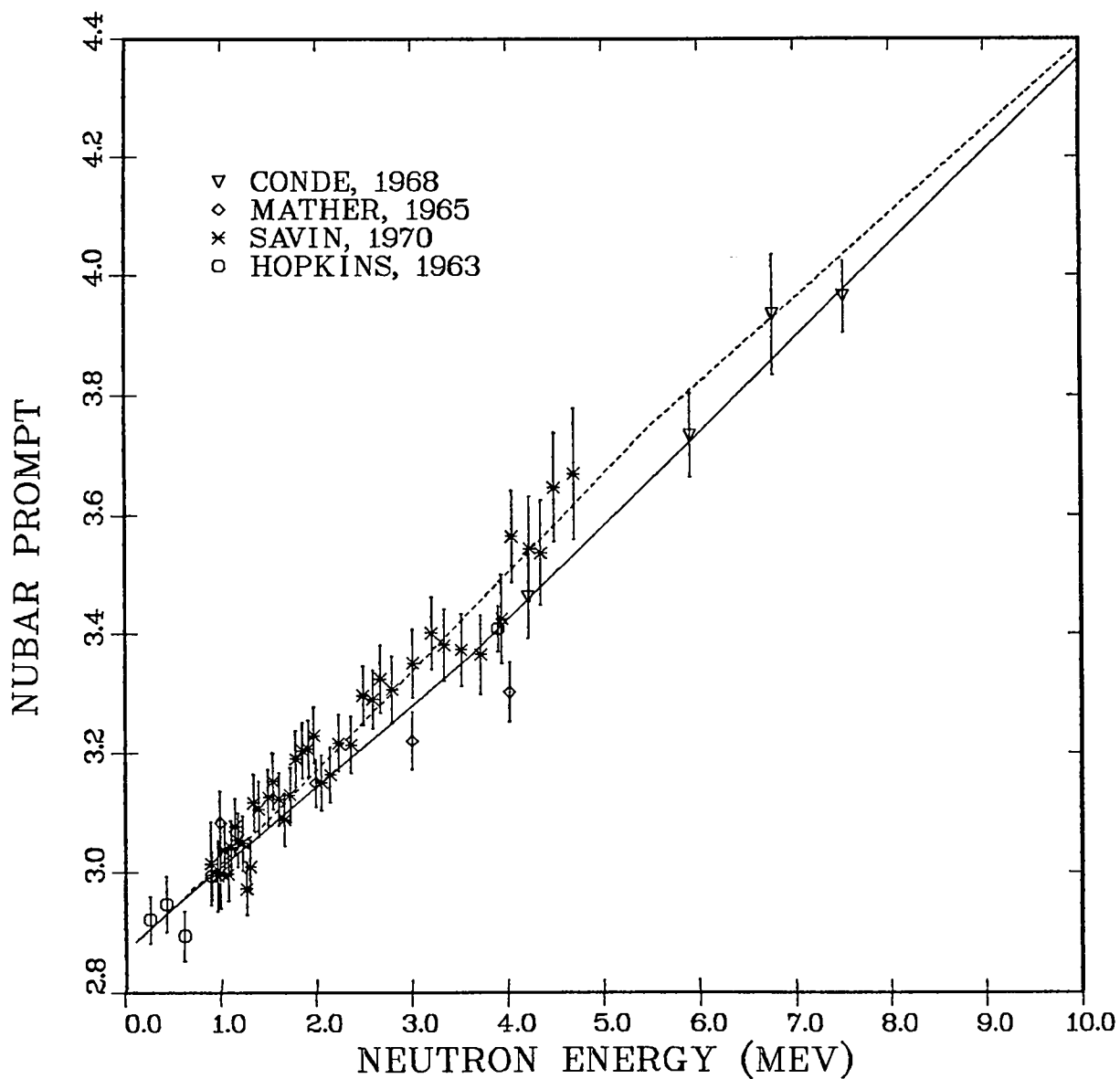


Fig. 15. Evaluated prompt fission multiplicity  $\bar{\nu}_p(E_n)$  between  $E_n = 0.1$  and 10 MeV compared with the experimental data of Condé et al.,<sup>39</sup> Mather et al.,<sup>38</sup> Savin et al.,<sup>36</sup> and Hopkins and Diven<sup>37</sup>. The curves are defined in the caption to Fig. 13.

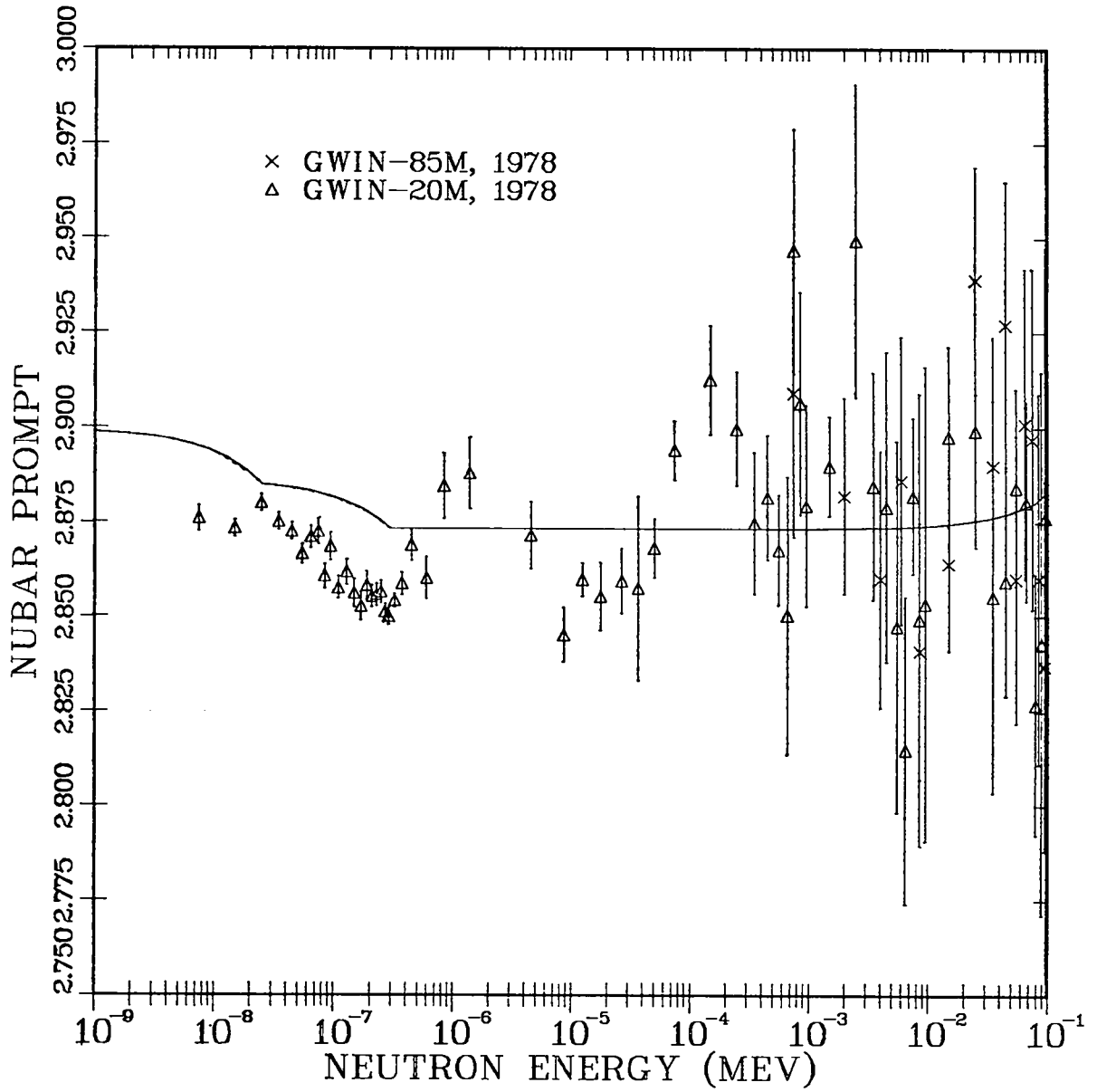


Fig. 16. Evaluated and experimental  $^{35}\bar{\nu}_p(E_n)$  for  $E_n = 0.001$  eV to 100 keV. The solid curve represents both ENDF/B-V and the present revision.

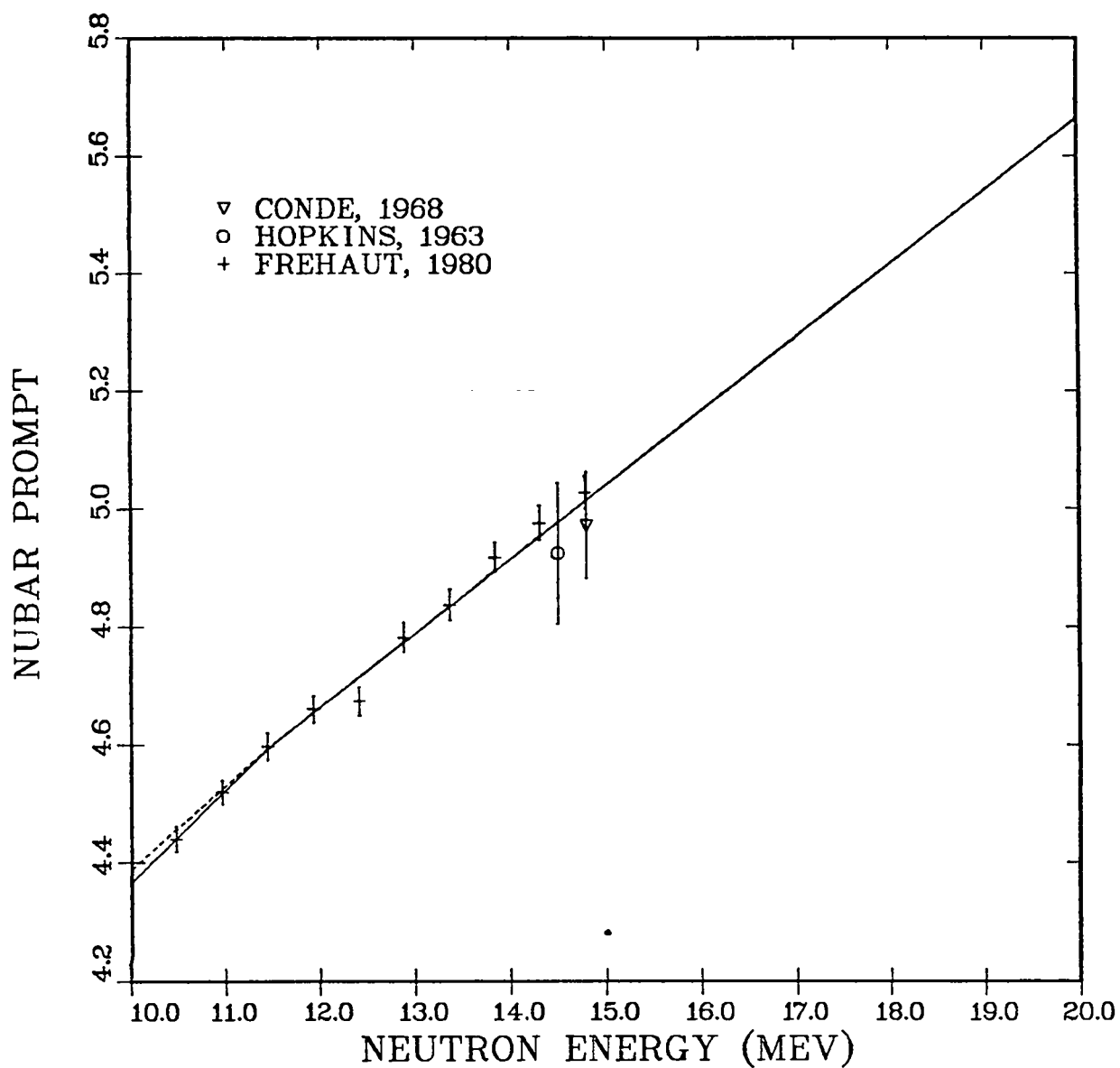


Fig. 17. Evaluated and experimental<sup>4,37,39</sup>  $\bar{\nu}_p(E_n)$  for  $E_n = 10$  to 20 MeV. The solid curve represents the present revision, and the dashed curve is ENDF/B-V.

This latter feature is obviously important for any applications sensitive to the high-energy tail of the fission spectrum.

The Madland-Nix formulation is based upon standard nuclear-evaporation theory and accounts for the physical effects of the motion of the fission fragments, the distribution of fragment excitation energy, and the energy dependence of the inverse process to neutron emission, namely, compound-nucleus formation. In general, the compound-nucleus formation cross section is a function of energy and is usually best determined from an optical model. Although the Madland-Nix theory reproduces experimental data best using an energy-dependent inverse cross section, good results can also be obtained with a constant inverse cross section if a suitable adjustment is made in the level density parameter. Because the constant inverse cross-section assumption permits an accurate, closed-form expression for the spectrum to be written, formats have been devised to directly accommodate this formulation in the ENDF/B system,<sup>41</sup> which we utilize in our analysis.

The basic equations for calculating the spectrum  $f(E \rightarrow E')$  of neutrons of energy  $E'$  due to first-chance fission induced by incident neutrons of energy  $E$  are as follows:

$$f(E \rightarrow E') = \frac{1}{2} [g(E', E_f^L) + g(E', E_f^H)] , \quad (1)$$

where

$$g(E', E_f) = \frac{1}{3(E_f T_m)^{1/2}} [u_2^{3/2} E_1(u_2) - u_1^{3/2} E_1(u_1) + \gamma(\frac{3}{2}, u_2) - \gamma(\frac{3}{2}, u_1)] . \quad (2)$$

In Eq. (2), the values of  $u_1$  and  $u_2$  are given by

$$u_1 = (\sqrt{E'} - \sqrt{E_f})^2 / T_m , \quad (3)$$

$$u_2 = (\sqrt{E'} + \sqrt{E_f})^2 / T_m ; \quad (4)$$



$E_1(x)$  is the exponential integral

$$E_1(x) = \int_x^{\infty} \frac{e^{-u}}{u} du ; \quad (5)$$

and  $\gamma(a,x)$  is the incomplete gamma function

$$\gamma(a,x) = \int_0^x u^{a-1} e^{-u} du . \quad (6)$$

The three basic input parameters required to calculate the first-chance fission spectrum are  $E_f^L$ ,  $E_f^H$ , and  $T_m$  in Eqs. 1-4. The quantities  $E_f^L$  and  $E_f^H$  are the average kinetic energies per nucleon of the average light and heavy fission fragments, respectively, and  $T_m$  is the maximum temperature of the fission-fragment residual nuclear-temperature distribution.

The constants  $E_f^L$  and  $E_f^H$  are assumed independent of incident neutron energy and can be determined from measurements of the total average fission-fragment kinetic energy<sup>42,43</sup> together with a knowledge of the fission-fragment mass distribution.<sup>42,43</sup> For the present evaluation, the values  $E_f^L = 1.0360$  MeV and  $E_f^H = 0.52857$  MeV were used, as determined in App. C of Ref. 5.

The  $T_m$  parameter is a function of incident neutron energy and depends on several fission-related quantities, on parameters of the compound fissioning nucleus, and on an effective level density parameter,  $a_{\text{eff}}$ . The scope of the present work did not permit thorough reevaluation of all fission spectrum measurements in terms of the Madland-Nix theory. Therefore, as an interim procedure, the parameter  $a_{\text{eff}}$  was simply adjusted so that the fission spectrum calculated for thermal incident neutrons resulted in the same average neutron energy as does ENDF/B-V. This value of  $a_{\text{eff}}$  was then used in the Madland-Nix theory to calculate  $T_m(E_n)$  up to the threshold for second-chance fission, defined to be 5.68 MeV in the evaluation. The  $T_m(E_n)$  at incident energies  $> 14$  MeV were determined by requiring the same average first-chance fission

neutron energy as is given by the ENDF/B-V evaluation. Between 5.68 and 14 MeV, the  $T_m$  points were joined by a linear line segment.

The fission neutron spectrum that results from thermal incident neutrons is compared in Fig. 18 with the ENDF/B-V evaluation. The solid curve is the ratio of the the present Madland-Nix spectrum to the Watt spectrum from Version V. Although both spectra result in the same average neutron energy ( $\langle E_n' \rangle = 2.1120$  MeV), there is a marked difference in the two above a secondary neutron energy of 8 MeV. At lower energies the ratio oscillates somewhat but never differs from unity by more than  $\pm 1.8\%$ .

The extension of the theory to include second-, third-, and fourth-chance fission requires a knowledge of the cross section for each of the multichance fission processes as well as the  $\bar{\nu}_p(E_n)$  appropriate for the various compound nuclei involved. The required equations are given in detail by Madland<sup>41</sup> and are not repeated here. For our calculations we adopted the multichance fission cross sections from ENDF/B-V and assumed that the neutron multiplicities are given by the approximation in Madland's Eq. (25), namely,

$$\nu_2(E_n - 2\theta_2 - B_2) = \nu_1(E_n) - 1 ,$$

$$\nu_3(E_n - 2\theta_2 - B_2 - 2\theta_3 - B_3) = \nu_1(E_n) - 2 ,$$

$$\nu_4(E_n - 2\theta_2 - B_2 - 2\theta_3 - B_3 - 2\theta_4 - B_4) = \nu_1(E_n) - 3 ,$$

together with the assumption that  $\nu_1(E_n) = \bar{\nu}_p(E_n)$ . The quantities  $\nu_i(E)$  are the average neutron multiplicities for each successive compound nucleus occurring in multichance fission, the  $\theta_i$  are neutron evaporation temperatures, and the  $B_i$  are neutron binding energies, as described in Ref. 41. Although the use of this approximation is not recommended in Ref. 41, it is appropriate here because of the large uncertainties in the ENDF/B-V multichance fission cross sections that we are using.

The temperatures  $T_m(E_n)$  for second-, third-, and fourth-chance fission were obtained from the first-chance fission values through the simple approximation

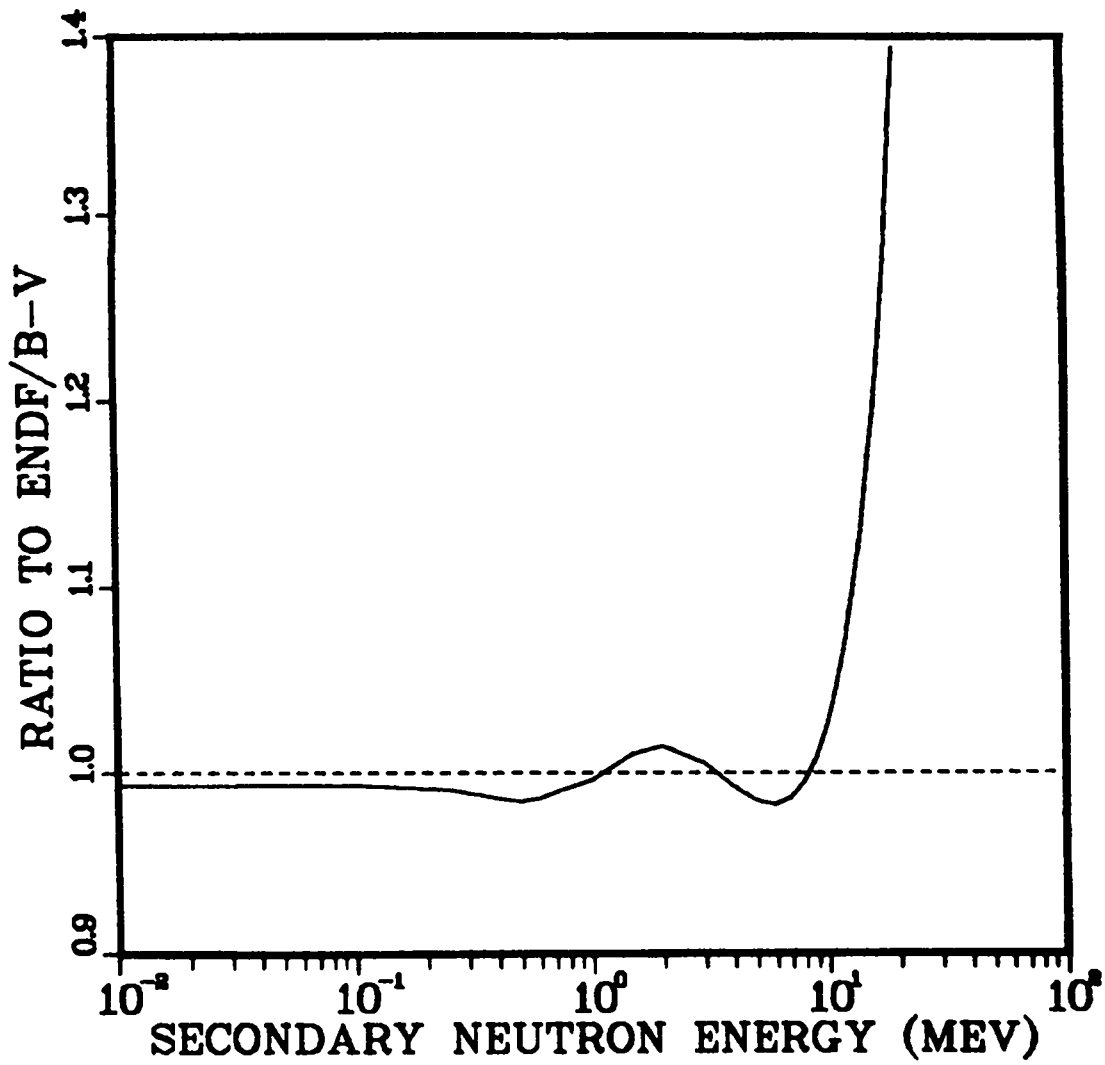


Fig. 18. Ratio of the revised fission neutron spectrum to ENDF/B-V (solid curve) for thermal incident neutrons.

$$T_m^{(2)}(E_n) = T_m(E_n - B_2) ,$$

$$T_m^{(3)}(E_n) = T_m(E_n - B_2 - B_3) ,$$

$$T_m^{(4)}(E_n) = T_m(E_n - B_2 - B_3 - B_4) .$$

That is, we assume the same  $T_m(E_n)$  curve for all the Pu isotopes, apart from a simple adjustment for the different excitation energies involved.

The average fission neutron energy that results from this treatment is plotted as a function of incident neutron energy (solid curve) in Fig. 19. Also shown are the ENDF/B-V values that result from total fission (ENDF/B reaction type MT=18; dashed curve) and from the sum of first-, second-, third-, and fourth-chance fission (MT=19,20,21,38; dotted curve). The dashed and dotted curves should in principle be the same, but an approximate form was used in ENDF/B-V to simplify the MT=18 representation. In the present evaluation, the total fission spectrum is consistent with the sum of the parts. The structure appearing in Fig. 19 corresponds to the onset of second-, third-, and fourth-chance fission and is determined by the fission-spectrum parameters we have assumed as well as the relative magnitudes of the multichance fission cross sections taken from ENDF/B-V.

Although a new ENDF/B-V format was devised (Law LF=12 in ENDF/B file MF=5) for directly inputting the Madland-Nix spectrum,<sup>41</sup> the Cross Section Evaluation Working Group only approved its use in official ENDF/B versions subsequent to Revision 2 of ENDF/B-V. Therefore, it was necessary to represent the new evaluation by a pointwise tabulation (LF=1 in MF=5) in the official ENDF/B-V, Revision 2 file. To accomplish this, an initial, unofficial data file was first constructed that makes use of LF=12 and includes a detailed description of the first-, second-, third-, and fourth-chance fission components as well as total fission. Tabulated fission spectra for the official Revision 2 evaluation were then computed from the total fission data in the unofficial version and appropriately formatted. Because of the length of the tabulations, however, only total fission (MT=18) is included in the official file. The unofficial file that employs LF=12 is

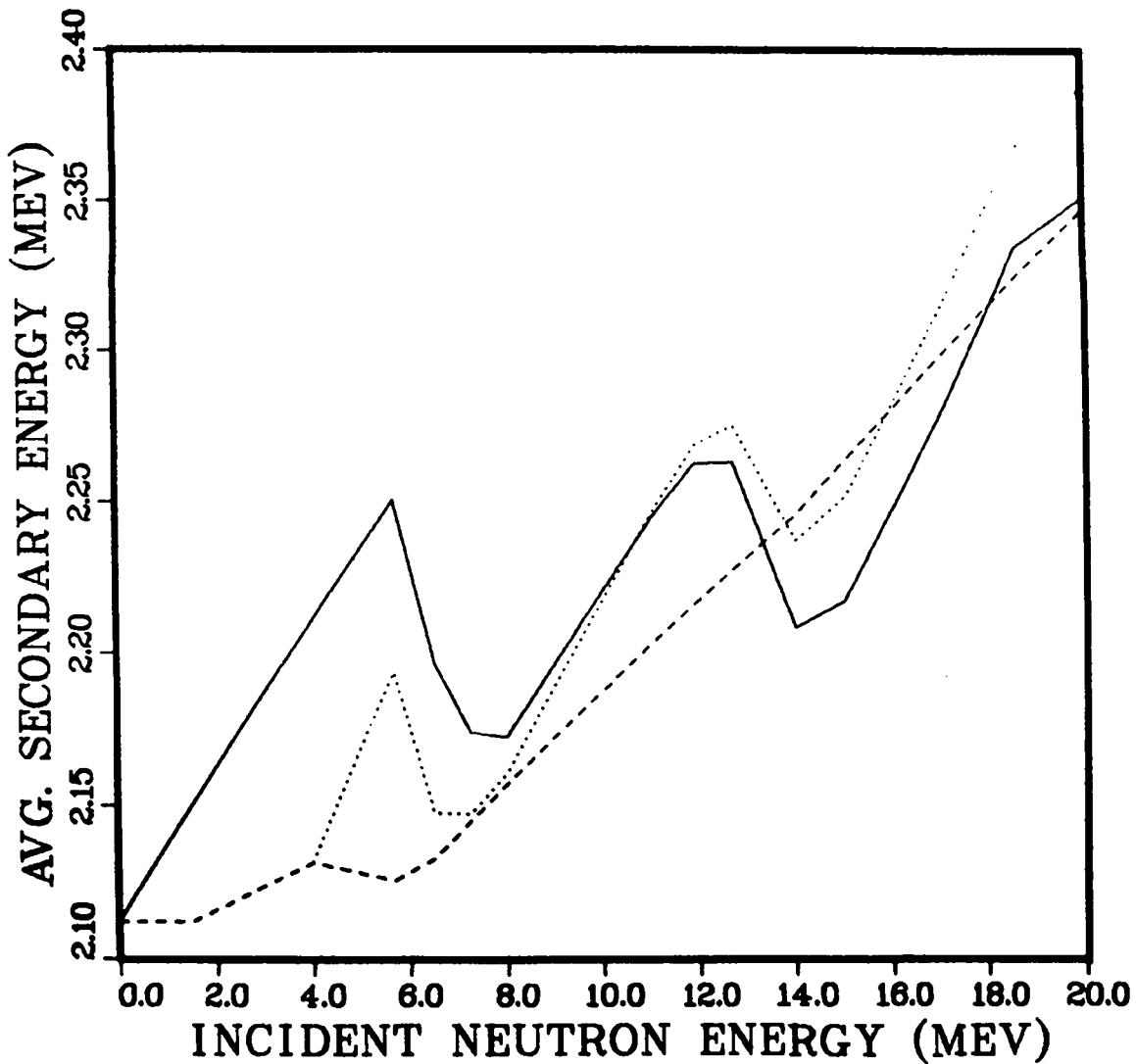


Fig. 19. Evaluated average secondary neutron energies from fission for incident neutron energies between 0 and 20 MeV. The solid curve is the present revision; the dashed curve is from MT=18 in ENDF/B-V; and the dotted curve is the sum of MT=19,20,21,38 in ENDF/B-V. See text for an explanation of the structure.

identical in every other respect to the official one and, in addition to preserving a more detailed fission description than the Revision 2 file, it is almost 1300 records shorter. The unofficial evaluation has been provided to the ENDF/A data library at the National Nuclear Data Center, Brookhaven National Laboratory.

Tabulated total fission neutron spectra are included at 19 incident energies in the Revision 2 evaluation. The qualitative effect of incident-energy interpolation is shown in Fig. 20, where the average secondary neutron energies from the tabulations (squares) are compared with a curve calculated on a fine grid from the unofficial evaluation that uses LF=12 in MF=5. The density of the tabulations is such that interpolation errors should be quite small in the first-chance fission region.

#### V. INTEGRAL TESTING WITH FAST CRITICAL MEASUREMENTS

After completion of the above revisions, calculations were made for five fast critical assemblies:<sup>44</sup> the bare plutonium sphere JEZEBEL (95%  $^{239}\text{Pu}$ ), the "dirty" plutonium sphere JEZEBEL-PU (20%  $^{240}\text{Pu}$ ), the uranium-reflected plutonium sphere FLATTOP-PU, the thorium-reflected plutonium sphere THOR, and the liquid-metal fast breeder reactor benchmark ZPR-6/7 (13%  $^{239}\text{Pu}$ ). Homogeneous, one-dimensional, spherical calculations were made using transport theory for the small assemblies and diffusion theory for ZPR-6/7. Eighty-group cross-section libraries based on the ENDF/B-V evaluation and both the "official" and "unofficial" versions of the present revision (see Sect. IV) were generated for each assembly using the TRANSX code<sup>45</sup> with MATXS libraries produced by the NJOY nuclear data processing system.<sup>46</sup> The official and unofficial representations of the Version V revision were found to give virtually identical results in the integral calculations.

The impact of the revisions to the ENDF/B-V evaluation is shown in Table III. The changes in the eigenvalue ( $k_{\text{eff}}$ ) and the  $^{238}\text{U}$  to  $^{235}\text{U}$  fission ratio ( $f^{28}/f^{25}$ ) are quite dramatic for the four small assemblies. The  $^{238}\text{U}$  fission ratios show a definite and consistent improvement, and the spread in the eigenvalues is reduced significantly. Only for the JEZEBEL-PU assembly was the eigenvalue calculation worsened, which might indicate problems with the

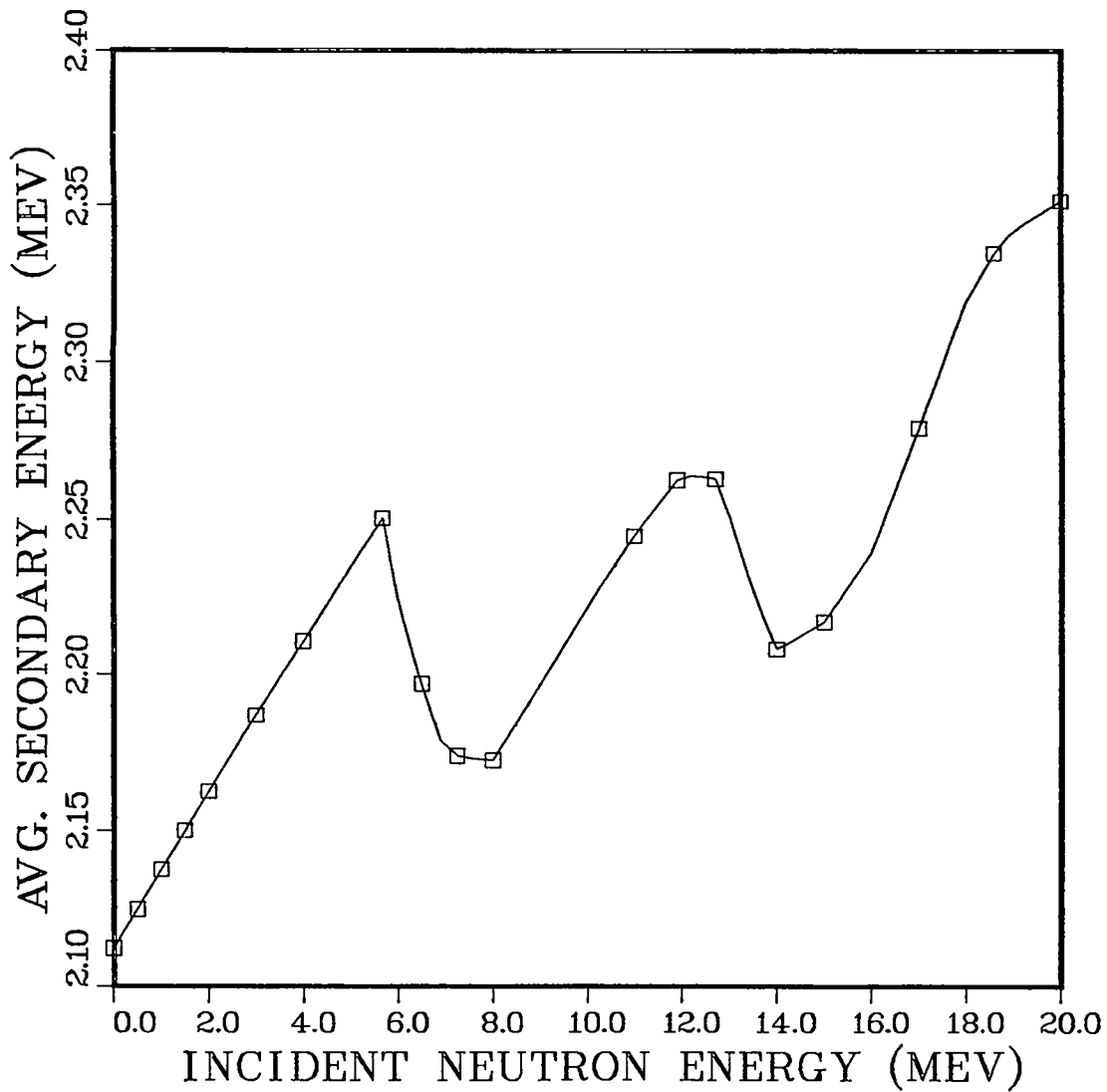


Fig. 20. Comparison of the average fission neutron energies from the tabulations in Revision 2 of ENDF/B-V (squares) with values computed from the unofficial version of the revision using the direct LF=12 representation<sup>41</sup> of the Madland-Nix formulation (solid curve). See text for an explanation of the structure.

TABLE III

CRITICAL ASSEMBLY PERFORMANCE PARAMETERS FOR  $^{239}\text{Pu}$ 

Parameter	ENDF/B-V	Revision 2	Assembly
$k_{\text{eff}}$	1.0068	0.9982	JEZEBEL <sup>c</sup>
$f_{28}/f_{25}$ (C/E) <sup>a</sup>	0.917	0.959	
$f_{23}/f_{25}$ (C/E)	0.987	0.985	
$f_{37}/f_{25}$ (C/E)	0.951	1.001	
$f_{49}/f_{25}$ (C/E)	0.972	0.975	
$f_{25}/f_{49}$ (C/E) <sup>b</sup>	1.028	1.026	
$f_{28}/f_{49}$ (C/E) <sup>b</sup>	0.943	0.984	
$k_{\text{eff}}$	0.9980	0.9917	JEZEBEL-PU <sup>c</sup>
$f_{28}/f_{25}$	0.923	0.958	
$f_{37}/f_{25}$	1.016	1.027	
$k_{\text{eff}}$	1.0179	1.0054	FLATTOP-PU <sup>c</sup>
$f_{28}/f_{25}$	0.920	0.965	
$f_{37}/f_{25}$	0.992	1.017	
$k_{\text{eff}}$	1.0228	1.0070	THOR <sup>c</sup>
$f_{28}/f_{25}$	0.901	0.948	
$f_{37}/f_{25}$	0.944	0.970	
$k_{\text{eff}}$	0.9956	0.9958	ZPR-6/7 <sup>d</sup>
$f_{25}/f_{49}$ (C/E)	1.018	1.018	
$f_{28}/f_{49}$ (C/E)	1.010	1.020	
$c_{28}/f_{49}$ (C/E)	1.078	1.077	
Average $k_{\text{eff}}$	1.008	1.000	
Spread in $k_{\text{eff}}$	0.025	0.015	

<sup>a</sup>Calculated result divided by the experimental result.

<sup>b</sup>Derived from benchmark's C/E values.

<sup>c</sup>Transport-corrected  $\text{P}_3\text{S}_{16}$  (with no other corrections).

<sup>d</sup>Diffusion theory with corrections specified for the benchmark.



$^{240}\text{Pu}$  data. The changes to ZPR-6/7 are smaller due to its lower  $^{239}\text{Pu}$  concentration and softer spectrum. In both cases, however, the changes to the inelastic cross section and fission neutron emission spectra have hardened the spectra of emitted neutrons. The calculated and measured leakage fluxes are shown explicitly for JEZEBEL in Table IV.

To investigate the sensitivity of the integral experiments to our revision of the fission spectrum, we reran the JEZEBEL and ZPR-6/7 calculations using the revised evaluation but with the original ENDF/B-V fission spectrum left unmodified. The percent changes in the various calculated quantities are given in Table V. In most cases, the changes are quite small. For JEZEBEL,  $k_{\text{eff}}$  becomes slightly worse when the ENDF/B-V spectrum is used, whereas the  $f^{25}/f^{49}$  C/E ratio is improved. The  $f^{28}/f^{49}$  C/E for JEZEBEL is virtually unchanged. The changes for ZPR-6/7 are very small, the largest being a 0.6% change in the C/E for  $f^{28}/f^{49}$  in the direction of improvement with the Version V spectrum.

## VI. CONCLUSIONS AND RECOMMENDATIONS

Significantly improved agreement with recent differential measurements was achieved by incorporating results from the new reaction theory analysis<sup>7</sup> into the  $^{239}\text{Pu}$  evaluation. Moreover, the improved physics in the analysis leads to increased confidence in  $(n,n')$  excitation cross sections and angular distributions at all incident energies, especially for high-lying and continuum levels where experimental data are lacking. The revision to the  $\bar{v}_p(E_n)$  data, while of an interim nature, does remove the serious discrepancy with experiment in the 2- to 10-MeV region that is evident for ENDF/B-V. The impact on the critical assembly calculations of the fission-spectrum revisions is not as great as the other modifications, but the spectrum change does embody a more realistic physical description and should improve the high-energy region of the fission spectrum. Applications such as deep penetration shielding calculations, dosimetry with threshold reactions, etc., can be sensitive to the high-energy tail of the fission spectrum. The combination of all the changes in the  $^{239}\text{Pu}$  evaluation substantially decreases discrepancies between measured and calculated results for hard critical

TABLE IV

## CALCULATED AND MEASURED LEAKAGE FLUX FROM JEZEBEL

Group	Experiment <sup>a</sup>	ENDF/B-V	Revision 2
1	3.1±0.5	2.4	2.4
2	11.7±0.7	9.8	10.3
3	17.7±0.7	17.6	18.3
4	20.0±0.8	20.0	20.0
5	16.5±0.7	18.4	17.7
6	13.6±0.7	14.3	13.6
7	9.7±0.7	9.4	9.0

<sup>a</sup>Leakage spectrum for one-half lethargy groups below 10 MeV, arbitrarily normalized to 20 for Group 4.

TABLE V

## SENSITIVITY OF CRITICAL PERFORMANCE PARAMETERS TO FISSION SPECTRUM

Parameter	% Difference <sup>a</sup>	Assembly
$k_{eff}$	-0.18	JEZEBEL
$f^{25}/f^{49}$	+0.10	
$f^{28}/f^{49}$	-1.6	
$k_{eff}$	-0.08	ZPR-6/7
$f^{25}/f^{49}$	+0.01	
$f^{28}/f^{49}$	-0.57	
$c^{28}/f^{49}$	+0.05	

<sup>a</sup>Revision 2 relative to Revision 2 with substitution of the ENDF/B-V fission spectrum.

assemblies such as JEZEBEL but has less effect on softer assemblies such as ZPR-6/7.

Although significant corrections are included in this interim evaluation, there are still several areas where improvements or more thorough analyses are needed for ENDF/B-VI. Some of the improvements that should be considered are

- a thorough, energy-dependent analysis of data in the thermal region, including data for other nuclei linked through ratio measurements as well as energy-dependent correlations in the data;
- a new analysis of the resolved and unresolved resonance regions that extends the resolved resonance region to as high an energy as feasible, that utilizes a multilevel formulation, and that includes the most recent experimental results;
- a thorough analysis of the smooth (n,f) and (n, $\gamma$ ) cross sections that accounts for energy correlations in the data and that incorporates ratio data and includes data for other nuclei linked through ratio measurements;
- a division of the total (n,f) cross section into multichance fission components based on a reaction theory analysis such as the one described here, and incorporation of (n,2n) and (n,3n) cross sections from such an analysis;
- inclusion of a variance-covariance analysis of  $\bar{\nu}_p(E_n)$  data that is properly meshed with the thermal analysis mentioned above; and
- a thorough incident-energy-dependent analysis of modern fission-spectrum measurements in terms of the Madland and Nix<sup>5</sup> formulation and inclusion of correct  $\bar{\nu}_p$  weighting in the spectrum calculations for multichance fission.

While it might not be feasible to implement all the above improvements, several of the recommended analyses are planned for Version VI of ENDF/B. Until such time that Version VI is available, however, the present interim evaluation offers significant improvements over ENDF/B-V.

#### REFERENCES

1. E. Kujawski, L. Stewart, and R. LaBauve, ENDF/B-V Data File for  $^{239}\text{Pu}$  (MAT 1399), described in BNL-NCS-17541, "ENDF-201: ENDF/B Summary Documentation," editor R. Kinsey, National Nuclear Data Center, Brookhaven National Laboratory, Upton, N. Y. (July 1979).
2. E. Kujawski, "Evaluation of the Pu-239 Data for ENDF/B-V," General Electric report GEFR-00247 (1977).
3. C. R. Weisbin, R. D. McKnight, J. Hardy, Jr., R. W. Roussin, R. E. Schenter, and B. A. Magurno, "Benchmark Data Testing of ENDF/B-V," Brookhaven National Laboratory report BNL-NCS-31531 (ENDF-311) (1982).
4. J. Frehaut, G. Mosinski, and M. Soleilhac, "Recent Results on Prompt Nubar Measurements between 1.5 and 15 MeV," communicated to the National Nuclear Data Center at Brookhaven National Laboratory in 1980, available as SCISRS accession number 20490.
5. D. G. Madland and J. R. Nix, "New Calculation of Prompt Fission Neutron Spectra and Average Prompt Neutron Multiplicities," Nucl. Sci. Eng. 81, 213 (1982).
6. E. D. Arthur, "Use of the Statistical Model for the Calculation of Compound Nucleus Contributions to Inelastic Scattering on Actinide Nuclei," Proc. Specialists Meeting on Fast Neutron Scattering on Actinide Nuclei, Paris, Nov. 23-25, 1981 [NEANDC-158"U" (1982)], p. 145.

7. E. D. Arthur, "Calculation of  $^{239}\text{Pu}$  Neutron Inelastic Cross Sections," Proc. Int. Conf. on Nuclear Data for Science and Tech., Antwerp, Sept. 6-10, 1982 [K. H. Böckhoff, Ed., Reidel Pub. Co., Dordrecht, Holland (1983)], p. 556.
8. C. I. Baxman and P. G. Young, Comp., "Applied Nuclear Data Research and Development: Jan. 1 - Mar. 31, 1981," Los Alamos National Laboratory report LA-8874-PR (1981).
9. P. G. Young, Comp., "Applied Nuclear Data Research and Development: Oct. 1, 1981 - Mar. 31, 1982," Los Alamos National Laboratory report LA-9468-PR (1982).
10. E. D. Arthur, Comp., "Applied Nuclear Data Research and Development: Apr. 1, 1982 - Sep. 30, 1982," Los Alamos National Laboratory report LA-9647-PR (1983).
11. E. D. Arthur, Comp., "Applied Nuclear Data Research and Development: Oct. 1, 1982 - Mar. 31, 1983," Los Alamos National Laboratory report LA-9841-PR (1983).
12. J. Raynal, "Optical Model And Coupled-Channel Calculations in Nuclear Physics," International Atomic Energy Agency report IAEA SMR-9/8 (1970).
13. C. M. Perey and F. G. Perey, "Compilation of Phenomenological Optical-Model Parameters: 1954-1975," At. Data and Nucl. Data Tables 17, 1 (1976).
14. G. Haouat, J. Lachkar, Ch. Lagrange, J. Jary, J. Sigaud, and Y. Patin, "Neutron Scattering Cross Sections for  $^{232}\text{Th}$ ,  $^{233}\text{U}$ ,  $^{235}\text{U}$ ,  $^{238}\text{U}$ ,  $^{239}\text{Pu}$ , and  $^{242}\text{Pu}$  between 0.6 and 3.4 MeV," Nucl. Sci. Eng. 81, 491 (1982).
15. W. P. Poenitz, J. F. Whalen, and A. B. Smith, "Total Neutron Cross Sections of Heavy Nuclei," Nucl. Sci. Eng. 78, 333 (1981).

16. C. L. Dunford, "A Unified Model for Analysis of Compound Nucleus Reactions," Atomic International report AI-AEC-12931 (1970).
17. P. G. Young and E. D. Arthur, "GNASH: A Preequilibrium, Statistical Nuclear-Model Code for Calculations of Cross Sections and Emission Spectra," Los Alamos Scientific Laboratory report LA-6947 (1977).
18. A. Gilbert and A. G. W. Cameron, "A Composite Nuclear-Level Density Formula with Shell Corrections," Can. J. Phys. 43, 1446 (1965).
19. J. L. Cook, H. Ferguson, and A. R. Musgrove, "Nuclear Level Densities in Intermediate and Heavy Nuclei," Aust. J. Phys. 20, 477 (1967).
20. D. M. Brink, thesis, Oxford University (1955).
21. P. Axel, "Electric Dipole Ground State Transition Width Strength Function," Phys. Rev. 126, 671 (1962).
22. S. F. Mughabghab and D. I. Garber, "Neutron Cross Sections, Volume 1, Resonance Parameters," Brookhaven National Laboratory report BNL-325, 3<sup>rd</sup> Ed., Vol. 1 (1973).
23. A. B. Smith and P. T. Guenther, "On the Neutron Inelastic-Scattering Cross Sections of  $^{232}\text{Th}$ ,  $^{233}\text{U}$ ,  $^{235}\text{U}$ ,  $^{238}\text{U}$ ,  $^{239}\text{Pu}$ , and  $^{240}\text{Pu}$ ," Argonne National Laboratory report ANL/NDM-63 (1982).
24. D. L. Hill and J. A. Wheeler, "Nuclear Constitution and the Interpretation of Fission Phenomena," Phys. Rev. 89, 1102 (1953).
25. B. B. Back, O. Hansen, H. C. Britt, and J. D. Garrett, "Fission of Doubly Even Actinide Nuclei Induced by Direct Reactions," Phys. Rev. C9, 1924 (1974).
26. J. E. Lynn and B. B. Back, "Sub-Barrier Fission Probability for a Double-Humped Barrier," J. of Phys. A71, 395 (1974).

27. H. C. Britt and J. B. Wilhelmy, "Simulated (n,f) Cross Sections for Exotic Actinide Nuclei," Nucl. Sci. Eng. 72, 222 (1979).
28. C. Budtz-Jørgensen, H. Knitter, and D. L. Smith, "Neutron-Induced Fission Cross Section of  $^{238}\text{Pu}$  in the Energy Range from 5 eV to 10 MeV," Proc. Int. Conf. on Nuclear Data for Science and Tech., Antwerp, Sept. 6-10, 1982 [K. H. Böckhoff, Ed., Reidel Pub. Co., Dordrecht, Holland (1983)], p. 206.
29. K. Kari and S. Cierjacks, "Measurement of the Fast Neutron Fission Cross Sections of  $^{239}\text{Pu}$  and  $^{240}\text{Pu}$ ," Int. Conf. on Neutron Physics and Nuclear Data for Reactors and Other Applied Purposes, Harwell, Sept. 25-29, 1978 (Organization for Economic Cooperation and Development, Paris, 1978) p. 206.
30. R. B. Schwartz, R. A. Schrack, and H. T. Heaton II, "Total Neutron Cross Sections of  $^{235}\text{U}$ ,  $^{238}\text{U}$ , and  $^{239}\text{Pu}$  from 0.5 to 15 MeV," Nucl. Sci. Eng. 54, 322 (1974).
31. A. B. Smith, P. Guenther, and J. Whalen, "Total and Elastic Scattering Neutron Cross Sections of  $^{239}\text{Pu}$ ," J. Nucl. En. 27, 317 (1973).
32. J. Frehaut, G. Mosinski, and M. Soleilhac, "Recent Results in  $\bar{\nu}_p$  Measurements between 1.5 and 15 MeV," European-American Nuclear Data Committee report EANDC(E)-154 (1973), p. 67.
33. M. Soleilhac, J. Frehaut, and G. Mosinski, "Recent Results in  $\bar{\nu}_p$  Measurements between 1.5 and 15 MeV," Proc. Second National Soviet Conf. on Neutron Physics, Kiev, May 28 - June 1, 1973 [Fiziko-Energeticheskij Institut, Kiev (1973)], p. 153.
34. M. Soleilhac, J. Frehaut, and J. Gauriau, "Energy Dependence of  $\bar{\nu}_p$  for Neutron-Induced Fission of  $^{235}\text{U}$ ,  $^{238}\text{U}$ , and  $^{239}\text{Pu}$  from 1.3 to 15 MeV," J. Nucl. En. 23, 257 (1969).

35. R. Gwin, R. R. Spencer, R. W. Ingle, J. H. Todd, and H. Weaver, "Measurements of the Average Number of Prompt Neutrons Emitted per Fission of  $^{239}\text{Pu}$  and  $^{235}\text{U}$ ," Oak Ridge National Laboratory report ORNL/TM-6246 (1978).
36. M. V. Savin, Ju. A. Khokhlov, Ju. S. Zamjatnin, and I. N. Paramonova, "The Average Number of Prompt Neutrons in Fast Neutron-Induced Fission of  $^{235}\text{U}$ ,  $^{239}\text{Pu}$ , and  $^{240}\text{Pu}$ ," Proc. Second IAEA Conf. on Nucl. Data for Reactors, Helsinki, June 15-19, 1970 [International Atomic Energy Agency, Vienna (1970)], V. II, p. 157.
37. J. C. Hopkins and B. C. Diven, "Prompt Neutrons from Fission," Nucl. Phys. 48, 433 (1963).
38. D. S. Mather, P. Fieldhouse, and A. Moat, "Measurement of Prompt  $\nu$  for the Neutron-Induced Fission of  $^{232}\text{Th}$ ,  $^{233}\text{U}$ ,  $^{234}\text{U}$ , and  $^{239}\text{Pu}$ ," Nucl. Phys. 66, 149 (1965).
39. H. Condé, J. Hansen, and M. Holmberg, "Prompt  $\bar{\nu}$  in Neutron-Induced Fission of  $^{239}\text{Pu}$  and  $^{241}\text{Pu}$ ," J. Nucl. Eng. 22, 53 (1968).
40. J. R. Stehn, M. Divadeenam, and N. E. Holden, "Evaluation of the Thermal Neutron Constants for  $^{233}\text{U}$ ,  $^{235}\text{U}$ ,  $^{239}\text{Pu}$ , and  $^{241}\text{Pu}$ ," Proc. Int. Conf. on Nuclear Data for Science and Tech., Antwerp, Sept. 6-10, 1982 [K. H. Böckhoff, Ed., Reidel Pub. Co., Dordrecht, Holland (1983)], p. 685.
41. D. G. Madland, "New Fission Neutron Spectrum Representation for ENDF," Los Alamos National Laboratory report LA-9285-MS (ENDF-321) (1982).
42. J. P. Unik, J. E. Gindler, L. E. Glendenin, K. F. Flynn, A. Gorski, and R. K. Sjoblom, "Fragment Mass and Kinetic Energy Distributions for Fissioning Systems Ranging from Mass 230 to 256," Proc. Third IAEA Sym. on Physics and Chemistry of Fission, Rochester, New York, Aug. 13-17, 1973 [International Atomic Energy Agency, Vienna (1974)], V. II, p. 19.



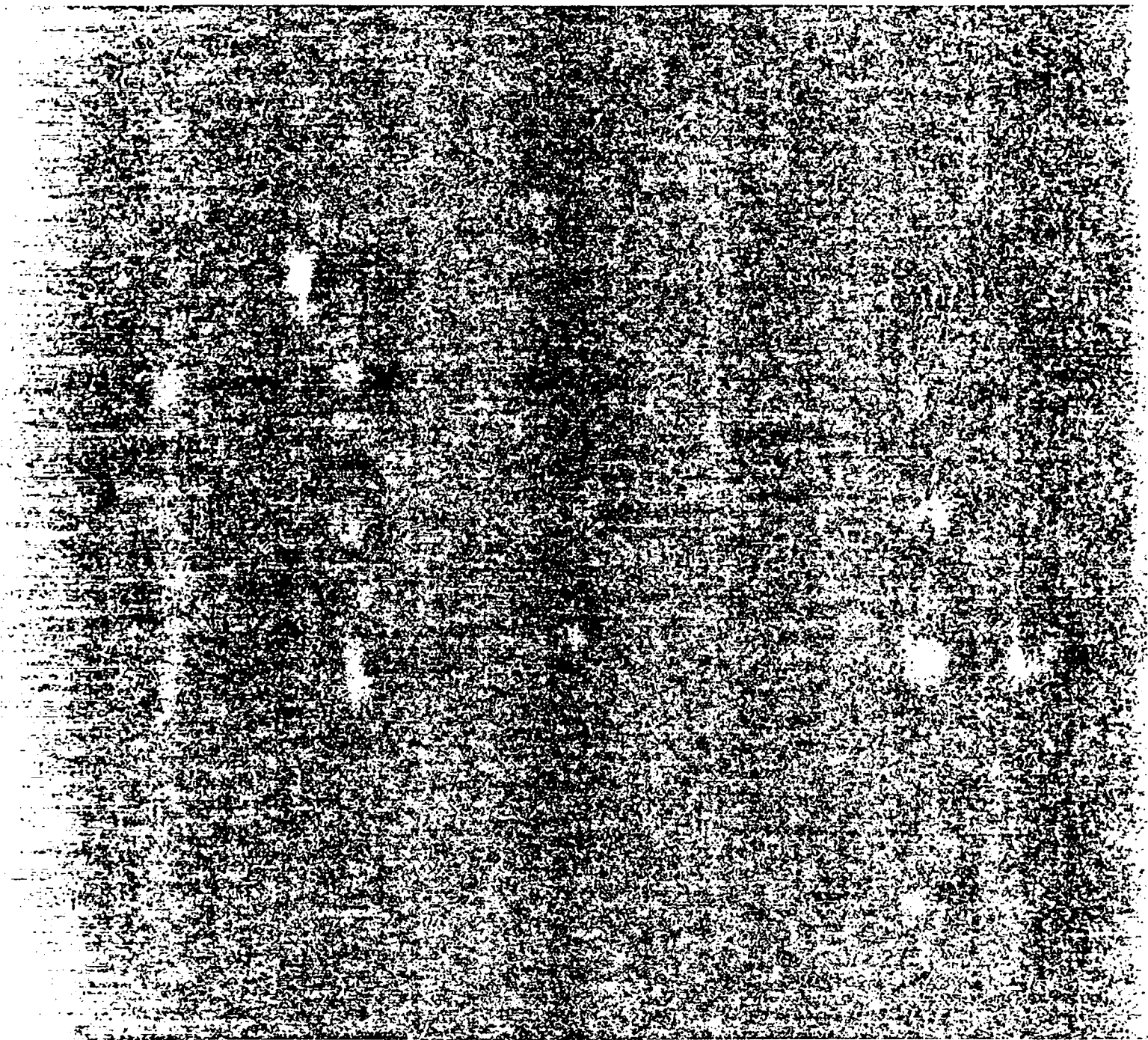
43. D. C. Hoffman and M. M. Hoffman, "Post-Fission Phenomena," Ann. Rev. Nucl. Nucl. Sci. 24, 151 (1974).
44. H. Alter, R. B. Kidman, R. J. LaBauve, R. Protsik, and B. A. Zolotar, "ENDF-202: Cross Section Evaluation Working Group Benchmark Specifications," Brookhaven National Laboratory report BNL-19302 (ENDF-202) (November 1974).
45. R. J. Barrett and R. E. MacFarlane, "The MATXS-TRANSX System and the CLAW-IV Nuclear Data Library," Proc. of Int. Conf. on Nuclear Cross Sections for Technology, Oct. 22-26, 1979, Knoxville, Tenn. (NBS Special Publication 594, 1980), p. 213.
46. R. E. MacFarlane, D. W. Muir, and R. M. Boicourt, "The NJOY Nuclear Data Processing System, Volume I: User's Manual," Los Alamos National Laboratory report LA-9303-M, Vol. I (ENDF-324) (1982).

Printed in the United States of America  
Available from  
National Technical Information Service  
US Department of Commerce  
5285 Port Royal Road  
Springfield, VA 22161

Microfiche (A01)

Page Range	NTIS Price Code	Page Range	NTIS Price Code	Page Range	NTIS Price Code	Page Range	NTIS Price Code
001-025	A02	151-175	A08	301-325	A14	451-475	A20
026-050	A03	176-200	A09	326-350	A15	476-500	A21
051-075	A04	201-225	A10	351-375	A16	501-525	A22
076-100	A05	226-250	A11	376-400	A17	526-550	A23
101-125	A06	251-275	A12	401-425	A18	551-575	A24
126-150	A07	276-300	A13	426-450	A19	576-600	A25
						601-up*	A99

\*Contact NTIS for a price quote.



Los Alamos